Synthesis, DFT Calculations to Investigate the Electronic Structure, Absorption Electronic Spectra, Antimicrobial Activity Application, and Non-Linear Optical Analysis of Pyridinyl and Pyrimidinyl Phosphonates Schemes

Abdel Halim, Shimaa*[+]

Department of Chemistry, Faculty of Education, Ain Shams University, Roxy 11711, Cairo, EGYPT

E. Ali, Tarik

Department of Chemistry, Faculty of Science, King Khalid University, Abha, SAUDI ARABIA

Abdel Kariem, Somaia M.

Department of Chemistry, Faculty of Education, Ain Shams University, Roxy 11711, Cairo, EGYPT

ABSTRACT: *In this paper, the structure optimized and calculations of the electronic properties for the study of two compounds which are **2** is Diethyl {5-[(2-hydroxy-5-methylphenyl) carbonyl] -2-thioxo-1,2,3,4-tetrahydropyrimidin-4-yl}-phosphonate (2), compound **4** is Diethyl {6-amino -1-(4-chlorophenyl) -5-cyano-3- [(2-hydroxy-5-methylphenyl)carbonyl] -1,2- dihydropyridin-2-yl]}phosphonate (4) have been performed by using the DFT method at the B3LYP/6-311++G (d, p) theory level. UV-Vis spectra, in both methanol and dioxane solvents, have been employed for two compounds **2** and **4** by density functional time-dependent theory (TD-DFT) calculations at the same level of calculation. The method of Coulomb-attenuating (CAM-B3LYP) and Corrected Linear Response Polarizable Continuum Model (CLR) PCM studied for theoretically obtaining the absorption electronic spectra in the gas phase, methanol, and dioxane, respectively; indicate a good agreement with the observed spectra and FT-IR, vibrational spectra were calculated. The GIAO method calculated the ^{1}H and ^{13}C NMR chemical shifts theoretically values which reflect better coincidence with the experimental chemical shifts. The dihedral angles result of calculations shows that two compounds 2 and 4 are non-planar. The stability of the two compounds 2 and 4, the hyper conjugative interactions, and the delocalization of the atomic charges was analyzed with the Natural Orbital Bond analysis (NBO). The relocation of electronic density and electronic structures were discussed. Studied functional density local descriptors, (MEP) Molecular Electrostatic Potential, molecular border orbitals, and absorption spectral. Analysis of the global descriptors revealed that compound 4 is the most reactive with an energy difference between the border orbital of ΔEgap = 3.605 eV. Furthermore, this compound 4 is the less stable, the softest, and has the greatest electronic exchange capacity of the other compound 2 studied. Studied by DFT calculations (SAR) structure-activity relationship and contacted with practical antimicrobial results for compounds 2 and 4.*

KEYWORDS: *UV-Vis spectra; DFT/TD-DFT; NBO and NLO analysis; Pyridinyl and pyrimidinyl phosphonates; FT-IR; Vibration analyses; NMR; Antimicrobial.*

***** *To whom correspondence should be addressed.*
+ *E-mail: Shimaaquantum@ymail.com*
1021-9986/2022/4/1250-1274 26/$/7.06

INTRODUCTION

Chromone derivatives have attracted considerable attention as very reactive compounds and can use as starting materials in the synthesis of strong two electrophilic centers with different series of heterocycles (the chromone system of carbon atoms C-2 and C-4) [1,2]. The highly polarized C2-C3p reactions bond with bi-nucleophiles occur predominantly via a nucleophilic attack on the accompanied ring-opening unsubstituted C2 atom (1,4-addition) and form the carbonyl intermediate, which can undergo intramolecular heterocyclization [3,4]. On the other hand, phosphonates are important organophosphorus compounds that possess various biological activities [5,6]. Some of these biological activities are antiproliferative [7], enzyme inhibitory [8] antibiotic [9], and antitumor [10]. In continuation of our interest in the synthesis and reactivity of new phosphonates containing different bioactive heterocyclic rings, we study here the structures of novel phosphonates containing pyridine and pyrimidine rings by theoretical methods.

Quantum theories of chemical reactivity currently make it possible to justify and/or predict rationally experimental region selectivity. The reactivity and selectivity predicting a chemical process are crucial. It is essentially based on two qualitative models which are the theory of border orbital and the conceptual DFT. Reactivity local to molecules and/or global descriptors has been an interest of to researchers in organic chemistry from Density Functional Theory (DFT) [11]. General chemical parameters such ionization potential (I / eV), electron affinity (A / eV), chemical hardness (η / eV), chemical potential (V / eV), electronegativity (χ /eV), and electrophilicity (ω/eV) and local reactivity descriptors such as local softness (S / eV). This is the framework for our previous work [12-14], which aims to study the properties of two compounds 2 and 4, and predict their applications. We provide a broad description of the chemical reactivity of two compounds 2 and 4 from the analysis of the Natural Bond Orbital (NBO) charge delocalization and chemical shift (NMR), FT-IR, Vibration analyses, DFT method was implemented of molecules were explored as well. The molecular modeling study with a hybrid quantum mechanical on this titled compound is not available. The structure and binding properties are new perceptions for this study. the electronic properties like the HOMO-LUMO energy gap, chemical hardness, and chemical potential. In addition, the Molecular Electrostatic Potential (MEP) and UV-Visible analyses were studied using theoretical calculations and experimental to provide spectra and structure electronic of pyridinyl and pyrimidinyl phosphonates compounds using CAM- B3LYP/6-311++G (d, p), Information on the charge transfer within each molecule. All calculations in this research have been done by using to DFT method at the B3LYP/6-311++G (d, P) theory level. Also, studied the relationship of structure-activity (SAR) by using the antimicrobial activity application for compounds 2 & 4.

EXPERIMENTAL SECTION

Synthesis Compounds

The structure of the two proposed molecules **2** and 4 of pyridinyl and pyrimidinyl phosphonates compounds, is shown below, where compound 2 is Diethyl {5-[(2-hydroxy-5-methylphenyl) carbonyl]-2-thioxo-1,2,3,4-tetrahydropyrimidin-4-yl} - phosphonate (2), compound 4 is Diethyl {6-amino-1-(4-chlorophenyl)-5-cyano-3-[(2-hydroxy-5-methylphenyl) carbonyl]-1,2-dihydropyridin-2-yl]}phosphonate (4).

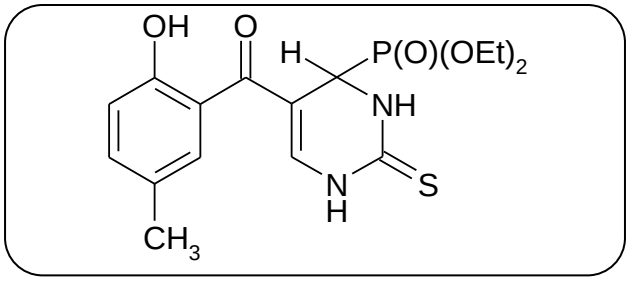

2

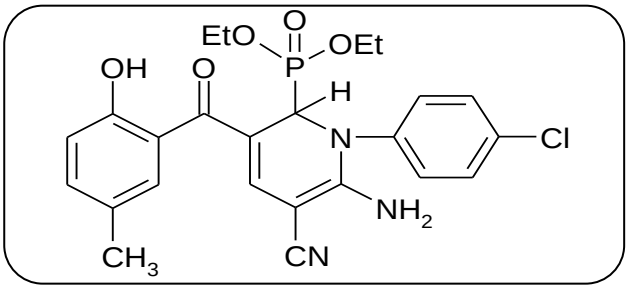

4

General procedure for the preparation of target compound 2

A mixture of 6-methyl-3-formylchromone (**1**) (5 mmol, 0.94 g), thiourea (5 mmol), and diethyl phosphite (10 mmol, 1.38 mL) was heated under reflux at 70−80 °C

for 2−8 hours. The reaction mixture was cooled then poured into ice and left for complete precipitation. The precipitate formed was filtered off, dried, and crystallized from ethanol.

Diethyl {5-[(2-hydroxy-5-methylphenyl) carbonyl]-2-thioxo-1,2,3,4-tetrahydropyrimidin-4-yl} - phosphonate (2)

Pale brown crystals from EtOH in 53 % yield; mp 196–198 °C. IR (KBr), (ν_{max}, cm^{-1}): 3293 (br, OH, NH), 3050 (C–H_{arom}), 2980, 2927 (C–H_{aliph}), 1641 (C=O), 1619 (C=C), 1214 (P=O), 1044 (P–O–C), 1165 (C=S). ^{1}H-NMR (300 MHz, DMSO–d_6): 1.08–1.36 (m, 6H, OCH_2CH_3), 2.28 (s, 3H, Ar–CH_3), 3.80–4.00 (m, 4H, OCH_2CH_3), 5.10 (d, 1H, *J*= 20 Hz, C***H***–P), 7.40–7.80 (m, 3H, Ar–***H*** and ***H***–6`$_{pyrimidine}$), 7.95 (s, 1H, Ar–***H***), 8.40 (brs, 1H, N***H*** exchangeable with D_2O), 9.10 (brs, 1H, N***H*** exchangeable with D_2O), 9.80 (brs, 1H, O***H*** exchangeable with D_2O). MS (EI, *m/z*): 384 (M^+). Anal. Calcd for $C_{16}H_{21}N_2O_5PS$ (384.39): C, 50.00; H, 5.51; N, 7.29; S, 8.33%. Found: C, 49.71; H, 5.24; N, 6.97; S, 7.97%.

General procedure for the preparation of target compound 4

A mixture of diethyl [(4-chlorophenylamino) (6-methyl-4-oxo-4*H*-chromen-3-yl)methyl]phosphonate (**4**) (2.30 mmol, 1 g) and malononitrile (2.30 mmol) in ethanolic sodium ethoxide solution (4.35 mmol, 0.10 g of sodium metal in 20 mL of absolute ethanol) was refluxed for 6−10 hours. The reaction mixture was cooled then poured into ice, neutralized with diluted hydrochloric acid (5%), and left for complete precipitation. The precipitate formed was filtered off, dried, and crystallized from methanol.

Diethyl {6-amino-1-(4-chlorophenyl)-5-cyano-3-[(2-hydroxy-5-methylphenyl) carbonyl]-1,2-dihydropyridin-2-yl]}phosphonate (4)

Orange crystals from methanol in 56% yield; mp 155−157 °C. IR (KBr), (ν_{max}, cm^{-1}): 3297 (br, OH and NH_2), 3050 (C–H_{arom}), 2983, 2917 (C–H_{aliph}), 2228 (C≡N), 1638 (C=O), 1593 (C=C), 1225 (P=O), 1025 (P–O–C). ^{1}H-NMR (300 MHz, DMSO–d_6): 1.14 (t, 3H, *J*= 7.8 Hz, OCH_2CH_3), 1.22 (t, 3H, *J*= 7.8 Hz, OCH_2CH_3), 2.30 (s, 3H, Ar–CH_3), 3.94 (q, 2H, *J*= 7.8 Hz, OCH_2CH_3), 4.04 (q, 2H, *J*= 7.8 Hz, OCH_2CH_3), 5.16 (dd, 1H, $^2J_{P–CH}$= 23.1 Hz and $^3J_{P–O–C}$= 8.7 Hz, C*H*–P), 6.44 (brs, 2H, NH_2 exchangeable with D_2O), 6.67 (d, 2H, *J*= 8.7 Hz, Ar−*H*), 7.06 (d, 2H, *J*= 8.7 Hz, Ar−*H*), 7.48 (d, 1H, *J*= 8.7 Hz, Ar−***H***), 7.60 (d, 1H, *J*= 7.2 Hz, Ar−***H***), 7.82 (s, 1H, Ar−***H***), 8.46 (s, 1H, ***H***−4$_{pyridine}$), 9.60 (s, 1H, O***H*** exchangeable with D_2O). ^{13}C-NMR (75 MHz, DMSO–d_6): 16.3 (OCH_2CH_3), 20.4 (CH_3), 45.9 (d, *J*= 150 Hz, C–P), 62.9 (OCH_2CH_3), 96.7 (***C***–5$_{pyridine}$), 106.1 (***C***≡N), 114.5 (***C***–2`,6`), 118.3 (***C***–3), 119.9 (***C***–1), 120.8 (***C***–3$_{pyridine}$), 122.2 (***C***–4`), 124.3 (***C***–4$_{pyridine}$), 128.2 (***C***–3`,5`), 128.6 (***C***–6), 130.0 (***C***–5), 135.6 (***C***–4), 145.5 (***C***–1`), 153.8 (***C***–2), 155.8 (***C***–6$_{pyridine}$), 182.5 (***C***=O). MS (EI, *m/z*): 504 (M+2), 502 (M^+). Anal. Calcd for $C_{24}H_{25}ClN_3O_5P$ (501.91): C, 57.43; H, 5.02; N, 8.37%. Found: C, 57.14; H, 5.30; N, 8.01%.

Solvents

Merck, AR- grade used methanol polar solvent and dioxane non-polar solvent without purification.

Apparatus

A Spectrophotometer using 1.0 cm fused quartz cells were used by A Perkin Elmer lambda 4B to measure the range 200-900 nm of the absorption electronic spectra.

A digital Stuart SMP3 apparatus was used for melting point determination. FT-IR Nicolet IS10 spectrophotometer (cm^{-1}) was applied to measure the Infrared spectra, using KBr disks. Mercury-300BB apparatus was used for measuring the ^{1}H NMR (300 MHz) and ^{13}C NMR (100 MHz) spectra, using DMSO-d_6 as a solvent and TMS (δ) as the internal standard. GC-2010 Shimadzu Gas chromatography instrument mass spectrometer (70 eV) was used for measuring the mass spectra. Elemental microanalyses were performed at PerkinElmer 2400II at the Chemical War Department, the Ministry of Defense, and Egypt. The purity of the synthesized compounds was checked by thin-layer chromatography and elemental microanalysis.

Antimicrobial Study

Biological activities of synthesized compounds 2 and 4 were studied for antibacterial and antifungal properties against different types of bacteria; Gram-positive- *S.* aureus, and *B. subtilis* and Gram-negative- *S. Typhimurium* and *E. Coli* also; *Yeast -C. albicans* for fungus. *A. fumigatus.*

Computational Details

The optimization of the geometry and the various parameters of quantum chemistry are carried out by the method of Density Functional Theory (DFT)

at the theoretical level B3LYP / 6-311++G (d, p) [15-17], it presents much fewer convergence problems than those commonly encountered for pure DFT methods. Therefore, the B3LYP method has been used in this document to perform quantum calculations using the Gaussian 09 program [18] and the Gauss View 5.0 [19] or chem craft 1.6 [20] software packages molecular visualization program. The total static dipole moment (μ), $\langle\Delta\alpha\rangle$, and $\langle\beta\rangle$, values were calculated from the literature [21-23]. The Time-Dependent-Density Functional Theory (TD-DFT) [24] calculated the maximum excitation wavelength (λ_{max}) and relative intensities (oscillator strengths, *f*), of the electronic transition properties, using "A new hybrid exchange-correlation functional using the Coulomb-attenuating method (CAM-B3LYP)," at the 6-311G (d, p) bases set [25].

Global Descriptors

PI = $-E_{HOMO}$, AE = $-E_{LUMO}$ calculates the energies of the border orbital within the framework of the validity of Koopmans' theorem [26]. HOMO and LUMO energies theorem relate to the ionization potential (PI) and electronic affinity (AE) respectively. Table 1 calculated the chemical hardness (η) = (PI-AE)/2, electronegativity (X) = (PI+AE)/2, chemical potential (V) = - (PI+AE)/2, electrophilicity (ω) = $\mu 2/ 2\eta$ and global softness (S) = $1/2\eta$ values. The molecule's ability to accept more electrons has the lowest LUMO value energy unoccupied molecular orbital. HOMO and LUMO energies, gap energy can be exploited to effectively predict the evolution of the reactivity and chemical stability of molecules 2 and 4. The energy gap (ΔE) lower value indicates a greater reactivity of the molecule and conversely low chemical stability.

NBO (Natural Bond Orbital)

Donor and acceptor types NBO intra and intermolecular interactions are presented in NBO analysis between (filled Lewis or binding NBO and empty Lewis NBO or anti-binder) and estimating their energy by second-order perturbation theory [27-28]. The stabilization energy $E^{(2)}$ [28] associated with the delocalization of electrons between the donor NBO (*i*) of electrons and the acceptor NBO (*j*), of electrons is evaluated according to the equation below.

$$E^{(2)} = \Delta E_{ij} = q_i \left(F(ij)^2 \big/ \varepsilon_j - \varepsilon_i \right)$$

$F(ij)$ is an element of the off-diagonal NBO Fock matrix, q_i represents the occupation of the donor orbital, ε_i and ε_j are the energies of the diagonal elements of NBO orbitals of the acceptor and the donor, respectively.

RESULT AND DISCUSSION

Chemistry

In recent years, much attention has been focused on the synthesis of phosphonate esters of N-heterocyclic systems (pyridine or pyrimidine) and their metal complexes, because of their potential applications and significant biological activities [29]. Thus, a fusion of 6-methyl-3-formylchromone (**1**) with thiourea in the presence of an excess of diethyl phosphite afforded diethyl {5- [(2-hydroxy-5-methyl phenyl) carbonyl]-2-thioxo-1,2,3,4-tetrahydropyrimidin-4-yl} phosphonate (2) in one-pot as the first type of pyrimidinyl phosphonate (Scheme 1) [30]. On the other hand, diethyl 6-amino-1-(4-chlorophenyl)-5-cyano-3- [(2-hydroxy-5-methyl phenyl) carbonyl]-1,2-dihydro-pyridin-2-yl] phosphonate (4) was obtained from refluxing of compound 3 with malononitrile in ethanolic sodium ethoxide (Scheme 2) [31]. Describing of construction and spectral characterization of the synthesized compounds 2 and 4 were reported in our recently published articles [30,31].

A mixture of 6-methyl-3-formylchromone (**1**) (5 mmol, 0.94 g), thiourea (5 mmol), and diethyl phosphite (10 mmol, 1.38 mL) was heated under reflux at 70−80 °C for 2−8 hours. The reaction mixture was cooled then poured into ice and left for complete precipitation. The precipitate formed was filtered off, dried, and crystallized from ethanol. Pale brown crystals from EtOH in 53 % yield; mp 196–198 °C. IR (KBr), (ν_{max}, cm^{-1}): (c.f. Fig. 1), 3293 (br, OH, NH), 3050 (C–H_{arom}), 2980, 2927 (C–H_{aliph}), 1641 (C=O), 1619 (C=C), 1214 (P=O), 1044 (P–O–C), 1165 (C=S).^{1}H-NMR (300 MHz, DMSO–d_6): (c.f. Fig. 3 and 4), 1.08–1.36 (m, 6H, $OCH_2C\boldsymbol{H}_3$), 2.28 (s, 3H, Ar–CH_3), 3.80–4.00 (m, 4H, OCH_2CH_3), 5.10 (d, 1H, *J*= 20 Hz, C*H*–P), 7.40–7.80 (m, 3H, Ar–*H* and *H*–6`$_{pyrimidine}$), 7.95 (s, 1H, Ar–*H*), 8.40 (brs, 1H, N*H* exchangeable with D_2O), 9.10 (brs, 1H, N*H* exchangeable with D_2O), 9.80 (brs, 1H, O*H* exchangeable with D_2O). MS (EI, *m/z*): (c.f. Fig. 7), 384 (M^+). Anal. Calcd for $C_{16}H_{21}N_2O_5PS$ (384.39): C, 50.00; H, 5.51; N, 7.29; S, 8.33%. Found: C, 49.71; H, 5.24; N, 6.97; S, 7.97%.

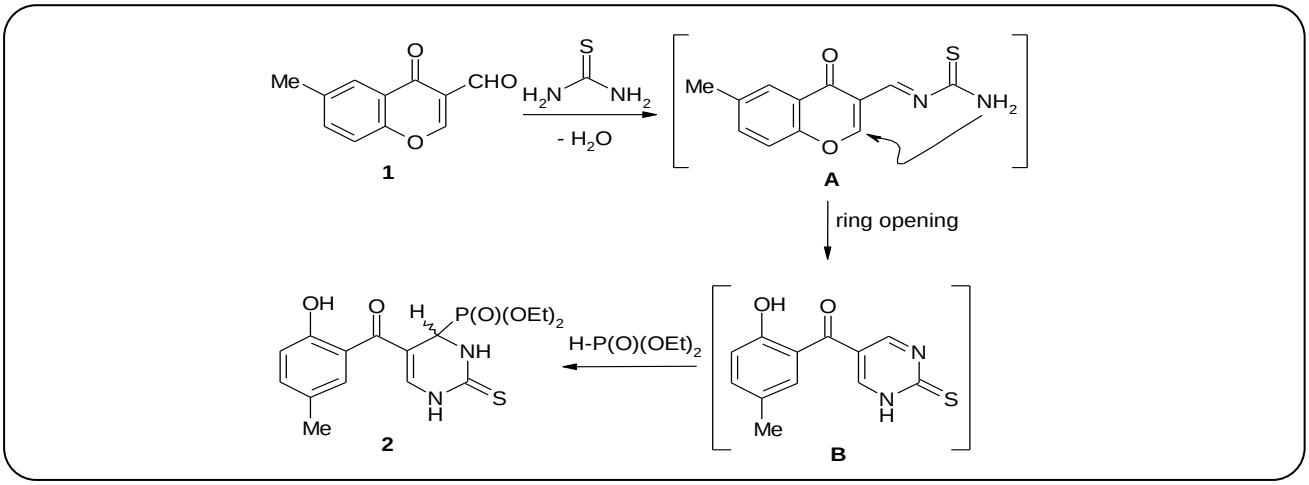

Scheme 1:

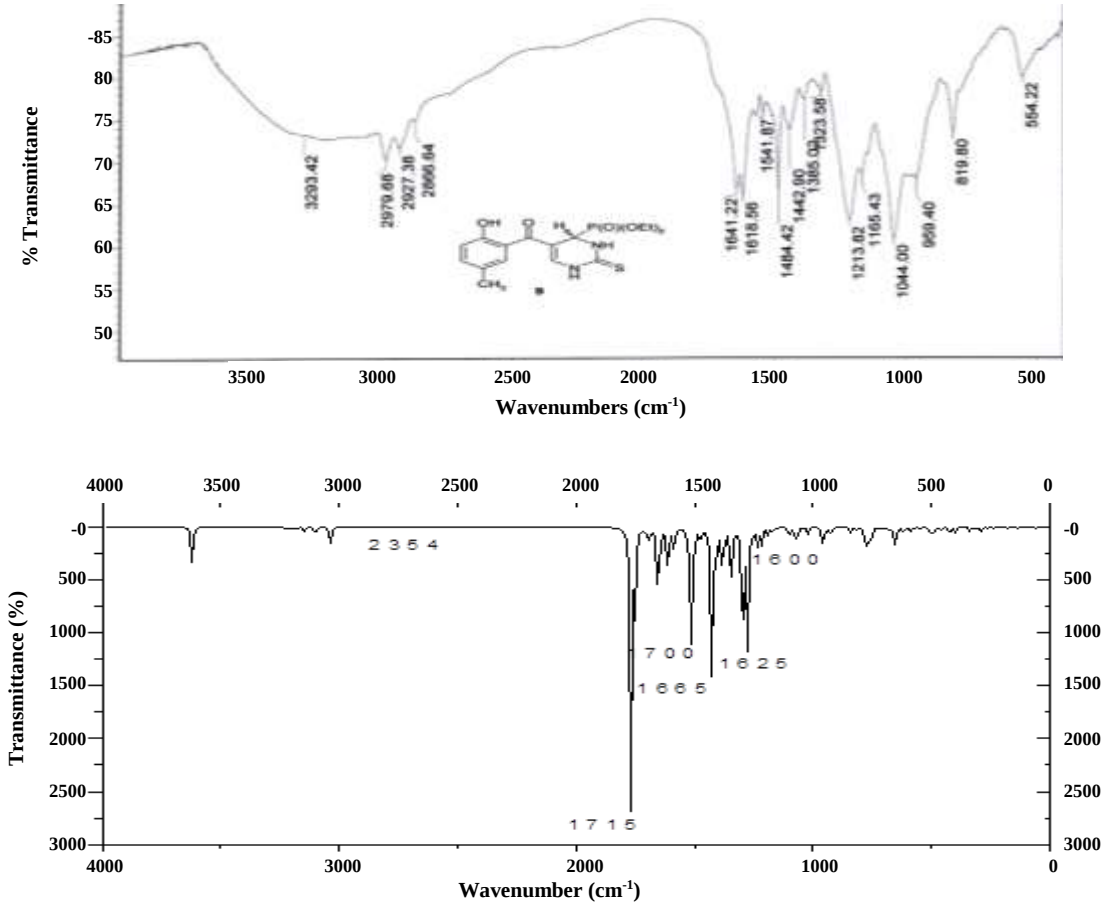

Fig. 1: Experimental and Calculated IR spectra for compound 2 at the B3LYP/6-311++G(d,p).

A mixture of diethyl [(4-chlorophenylamino) (6-methyl-4-oxo-4*H*-chromen-3-yl) methyl]phosphonate (**4**) (2.30 mmol, 1 g) and malononitrile (2.30 mmol) in ethanolic sodium ethoxide solution (4.35 mmol, 0.10 g of sodium metal in 20 mL of absolute ethanol) was refluxed for 6−10 hours. The reaction mixture was cooled then poured into ice, neutralized with diluted hydrochloric acid (5%), and left for complete precipitation. The precipitate formed

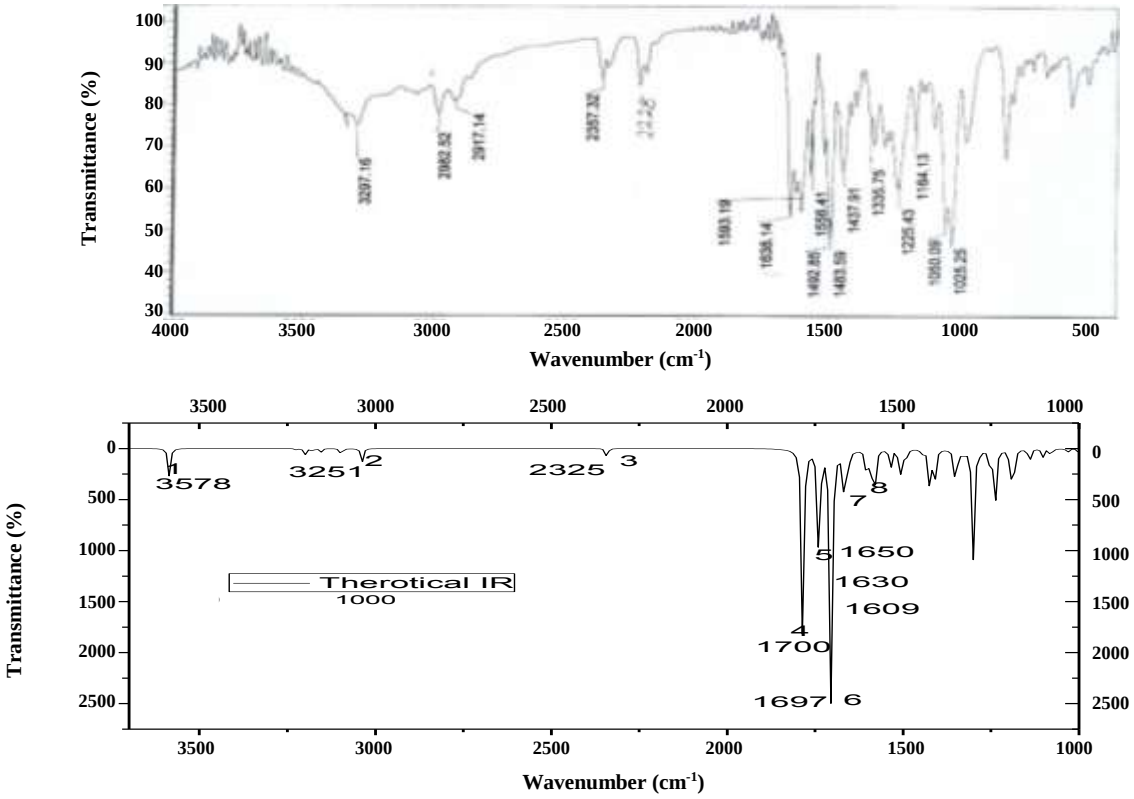

Fig. 2: Experimental and Calculated IR spectra for compound 4 at the B3LYP/6-311++G (d, p).

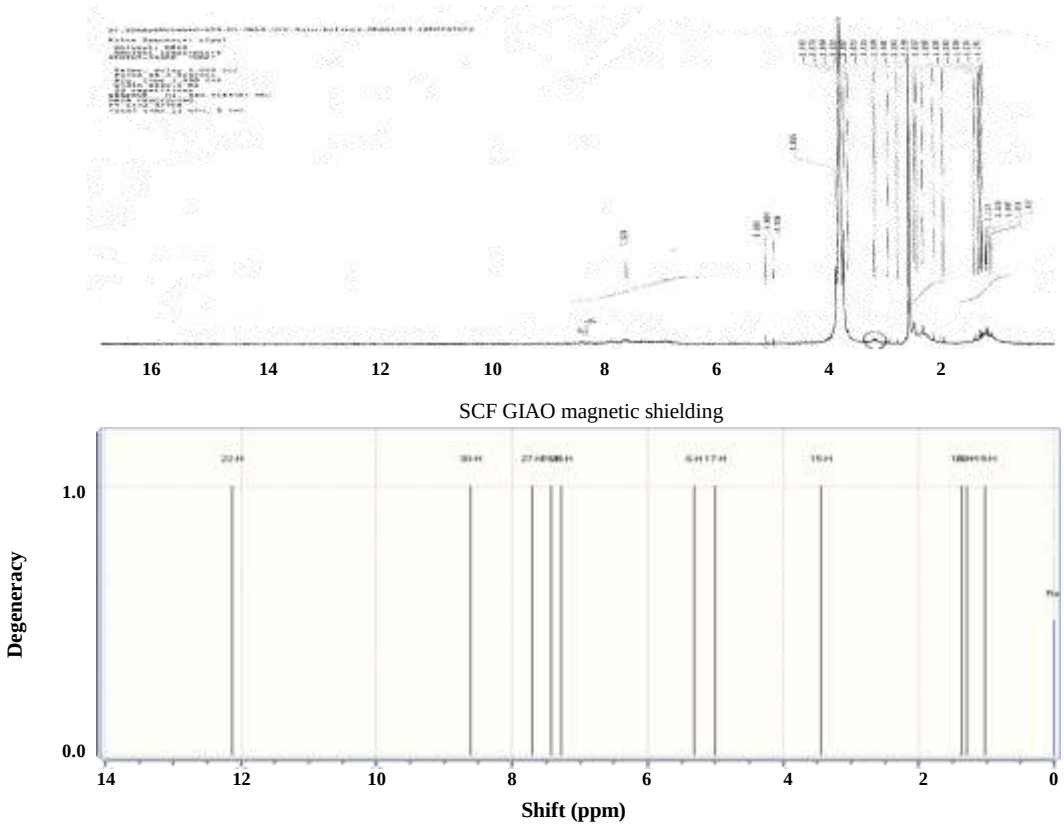

Fig. 3: The ^{1}H NMR spectrum Theoretical and Experimental of compound 2.

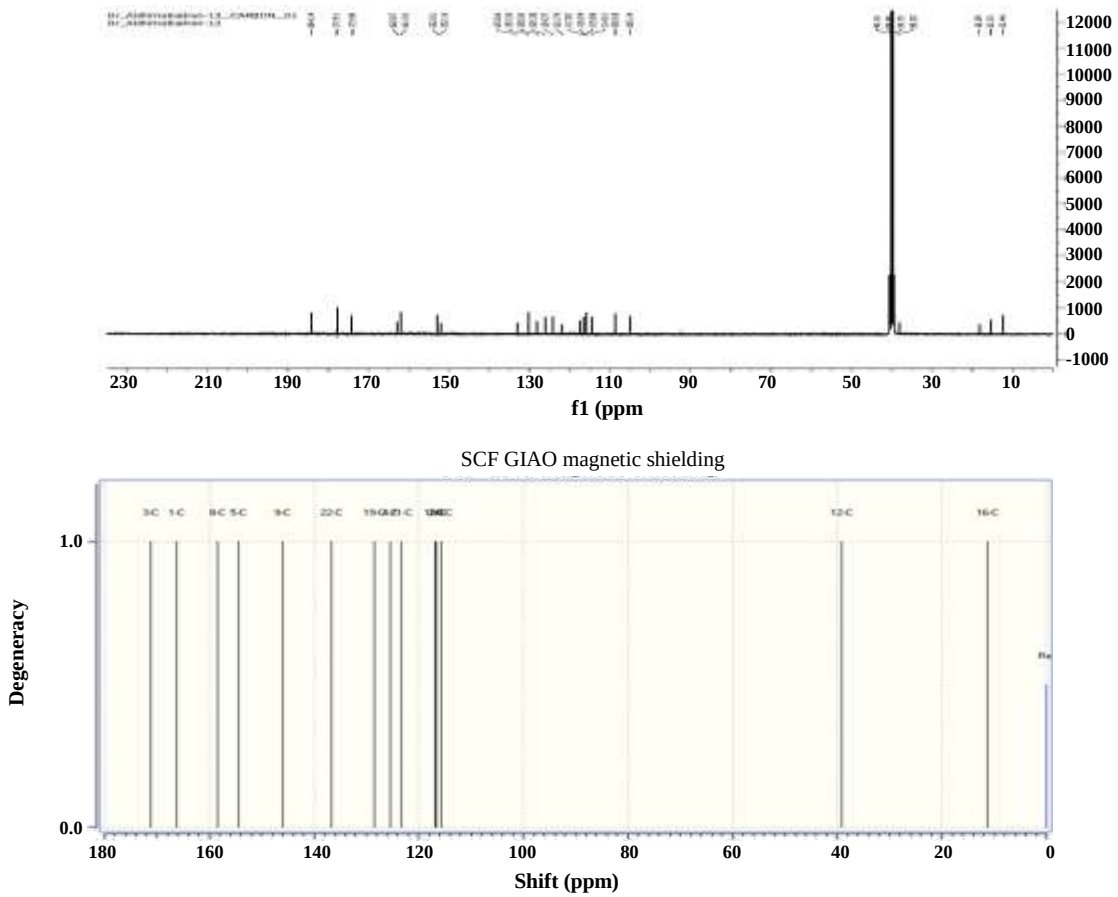

Fig. 4: The ^{13}C NMR spectrum Thermotical and Experimental of compound 2.

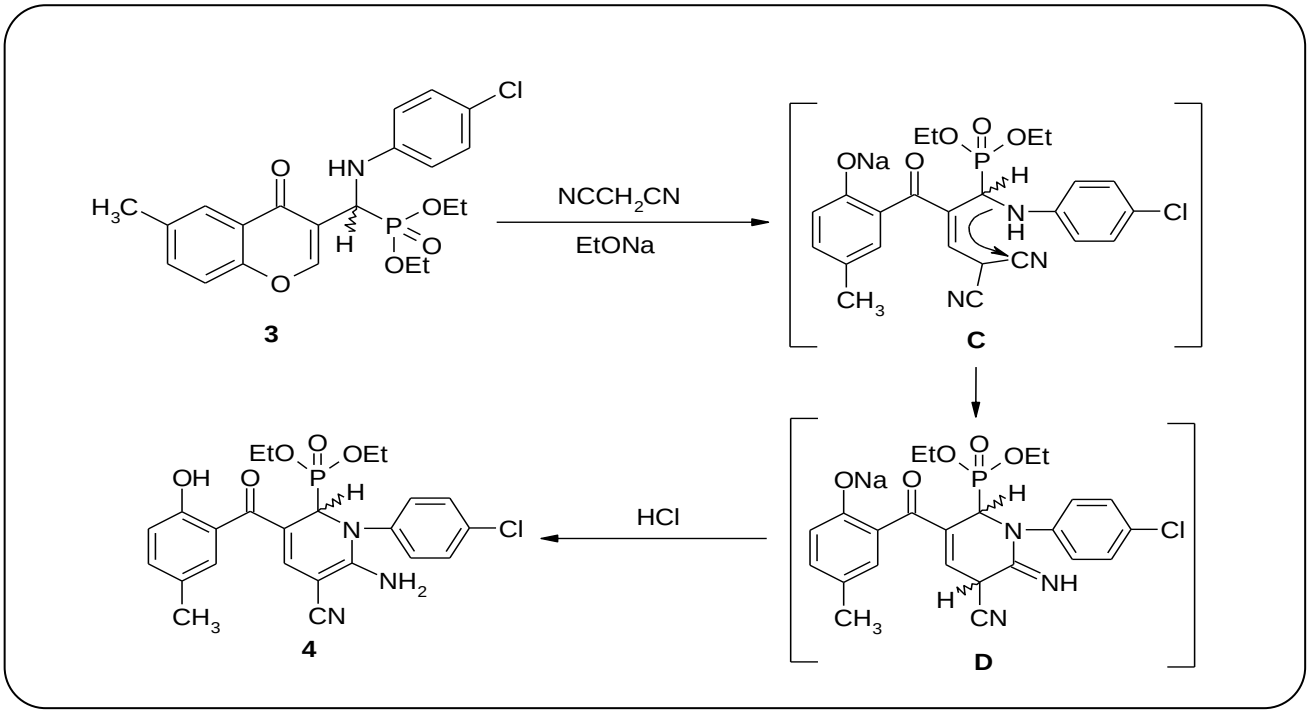

Scheme 2:

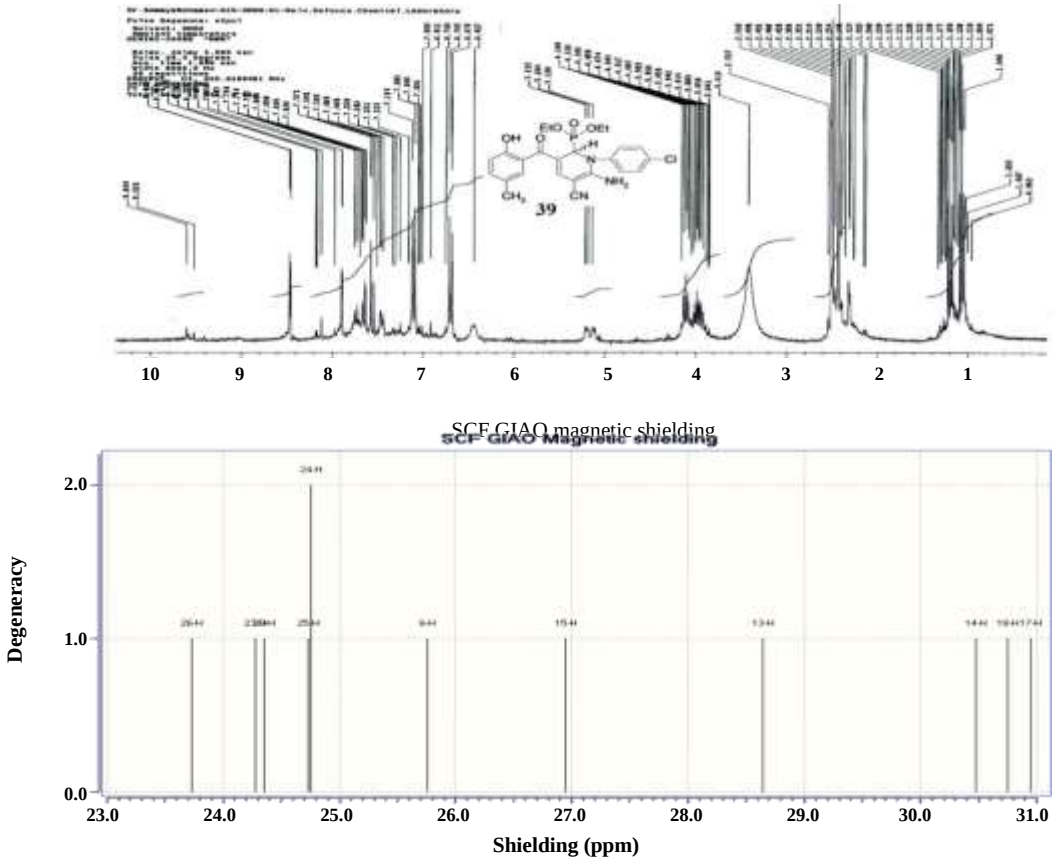

Fig. 5: The ^{1}H NMR spectrum Theoretical and Experimental of compound 4.

was filtered off, dried, and crystallized from methanol. Orange crystals from methanol in 56% yield; mp 155−157 ºC. IR (KBr), (ν_{max}, cm^{-1}): (c.f. Fig. 2), 3297 (br, OH and NH_2), 3050 (C–H_{arom}), 2983, 2917 (C–H_{aliph}), 2228 (C≡N), 1638 (C=O), 1593 (C=C), 1225 (P=O), 1025 (P–O–C). ^{1}H-NMR (300 MHz, DMSO–d_6): (c.f. Fig. 5), 1.14 (t, 3H, *J*= 7.8 Hz, OCH_2CH_3), 1.22 (t, 3H, *J*= 7.8 Hz, OCH_2CH_3), 2.30 (s, 3H, Ar–CH_3), 3.94 (q, 2H, *J*= 7.8 Hz, OCH_2CH_3), 4.04 (q, 2H, *J*= 7.8 Hz, OCH_2CH_3), 5.16 (dd, 1H, $^2J_{P–CH}$= 23.1 Hz and $^3J_{P–O–C}$= 8.7 Hz, C*H*–P), 6.44 (brs, 2H, NH_2 exchangeable with D_2O), 6.67 (d, 2H, *J*= 8.7 Hz, Ar−*H*), 7.06 (d, 2H, *J*= 8.7 Hz, Ar−*H*), 7.48 (d, 1H, *J*= 8.7 Hz, Ar−*H*), 7.60 (d, 1H, *J*= 7.2 Hz, Ar−*H*), 7.82 (s, 1H, Ar−*H*), 8.46 (s, 1H, *H*−$4_{pyridine}$), 9.60 (s, 1H, O*H* exchangeable with D_2O). ^{13}C-NMR (75 MHz, DMSO–d_6): (c.f. Fig. 6), 16.3 (OCH_2CH_3), 20.4 (CH_3), 45.9 (d, *J*= 150 Hz, *C*H–P), 62.9 (OCH_2CH_3), 96.7 (*C*–$5_{pyridine}$), 106.1 (*C*≡N), 114.5 (*C*–2`,6`), 118.3 (*C*–3), 119.9 (*C*–1), 120.8 (*C*–$3_{pyridine}$), 122.2 (*C*–4`), 124.3 (*C*–$4_{pyridine}$), 128.2 (*C*–3`,5`), 128.6 (*C*–6), 130.0 (*C*–5), 135.6 (*C*–4), 145.5 (*C*–1`), 153.8 (*C*–2), 155.8 (*C*–$6_{pyridine}$), 182.5 (*C*=O). MS (EI, *m/z*): (c.f. Fig. 8), 504 (M+2), 502 (M^+). Anal. Calcd for $C_{24}H_{25}ClN_3O_5P$ (501.91): C, 57.43; H, 5.02; N, 8.37%. Found: C, 57.14; H, 5.30; N, 8.01%.

Electronic structures

Geometry structure

Figs. (9-11) and Table (1) show geometrical optimized and ground state energies of compounds 2 and 4 obtained using the B3LYB/6-311++G (d, p) level. From the analysis clear that: The optimized bond length of C=C in the phenyl ring falls in the range from 1.360 to 1.479A^0 which are in good agreement with the experimental data 1.481A^0, [32] for C=O bonds, the optimized length obtained by B3LYB/6-311++G (d, p) is slightly longer than the experimental data 1.229A^0, [32]. The computed bond angles are largely affected by the presence of the C=O group in C4 and C18, in two compounds 2 and 4, especially <C4C8O9 in compound 2 is 120.26º and compound 4 is 119.34º also; <C18C8O9 in compound 2 is 117.34º and compound 4 is 125.98º, respectively. (Fig.10). The most stable geometry of the studied compounds 2 and 4 is the non-planar structure.

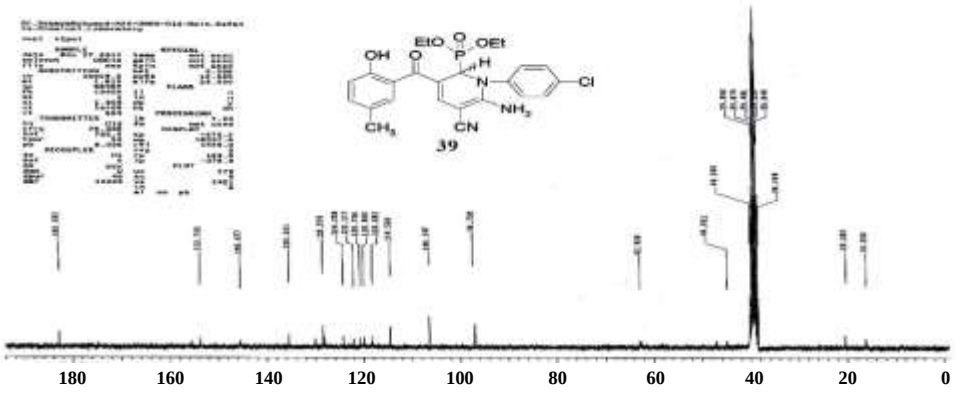

Fig. 6: The ^{13}C NMR spectrum Thermotical and Experimental of compound 4.

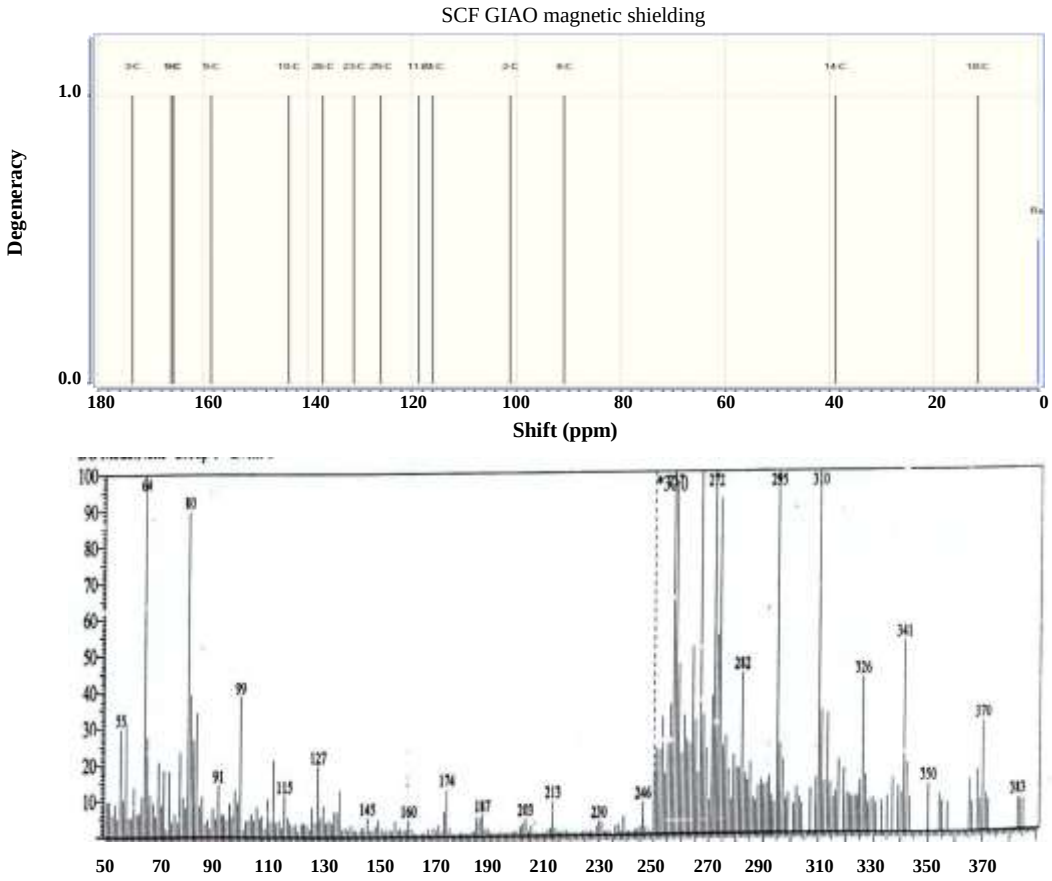

Fig. 7: The mass spectrum of (2).

Global reactivity descriptors and Ground state properties

The study of the global chemical reactivity of molecules is based on the calculation of global indices deduced from electronic properties. The global descriptors of chemical reactivity of the studied compounds **2** and **4**, the Ionization Energy (I.E) which measures the donating property (oxidation power), the Electron Affinity (E.A) which measures the accepting property (reducing power), the polarity or charge separation measurement theoretically by computed dipole moment (μ), are given in Fig. 11 and Table 1. The analysis in Table 1 shows that compound **4** which has the lowest energy difference values (ΔE = 3.60 eV) is the most reactive and less stable molecule. Thus, the following sequence can be established in order of

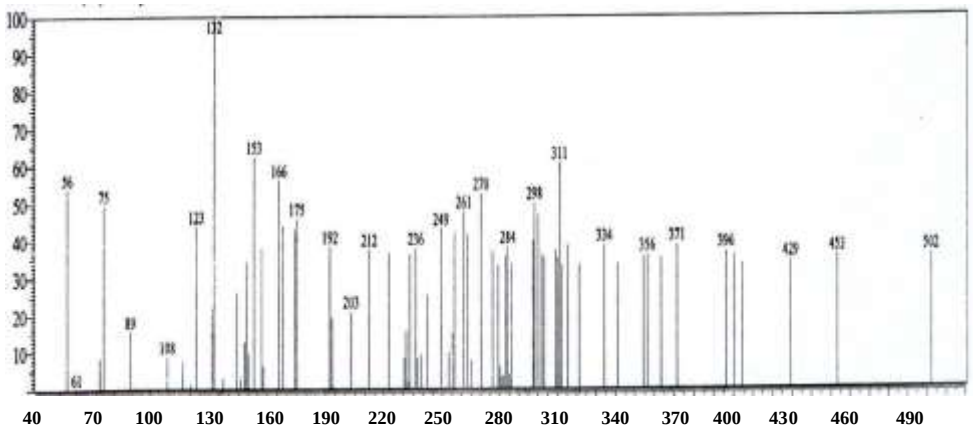

Fig. 8: The mass spectrum of (4).

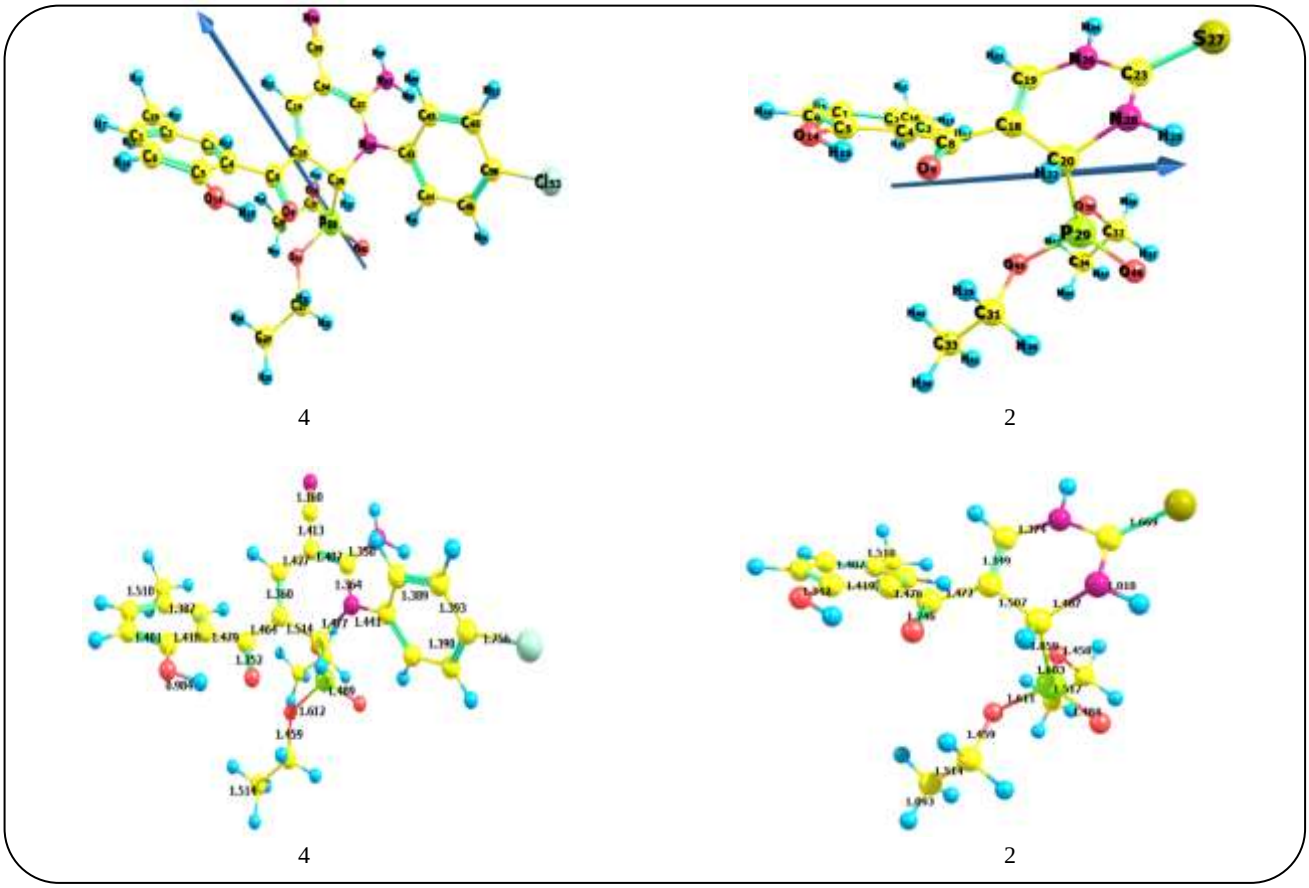

Fig. 9: Optimized geometry, numbering system, vector of dipole moment, and bond length of compounds 2 and 4 using B3LYP/6-311++G(d,p).

decreasing reactivity: ΔE: **4** > **2**. The other descriptor analyzed is the chemical hardness (η), always compound **4** having the lowest value (1.8025 eV) to that of the other compound **2** indicating that it is the softest among the other compound **2** was studied. Furthermore, this compound **4** has the greatest electronic exchange capacity with the highest value of electronegativity (*X*), or chemical potential (V) (± 3.9628 eV). In summary, the global descriptors revealed that compound 4 is the most reactive, the less stable, and the softest and it has the greatest electronic exchange capacity of the other compound 2 studied.

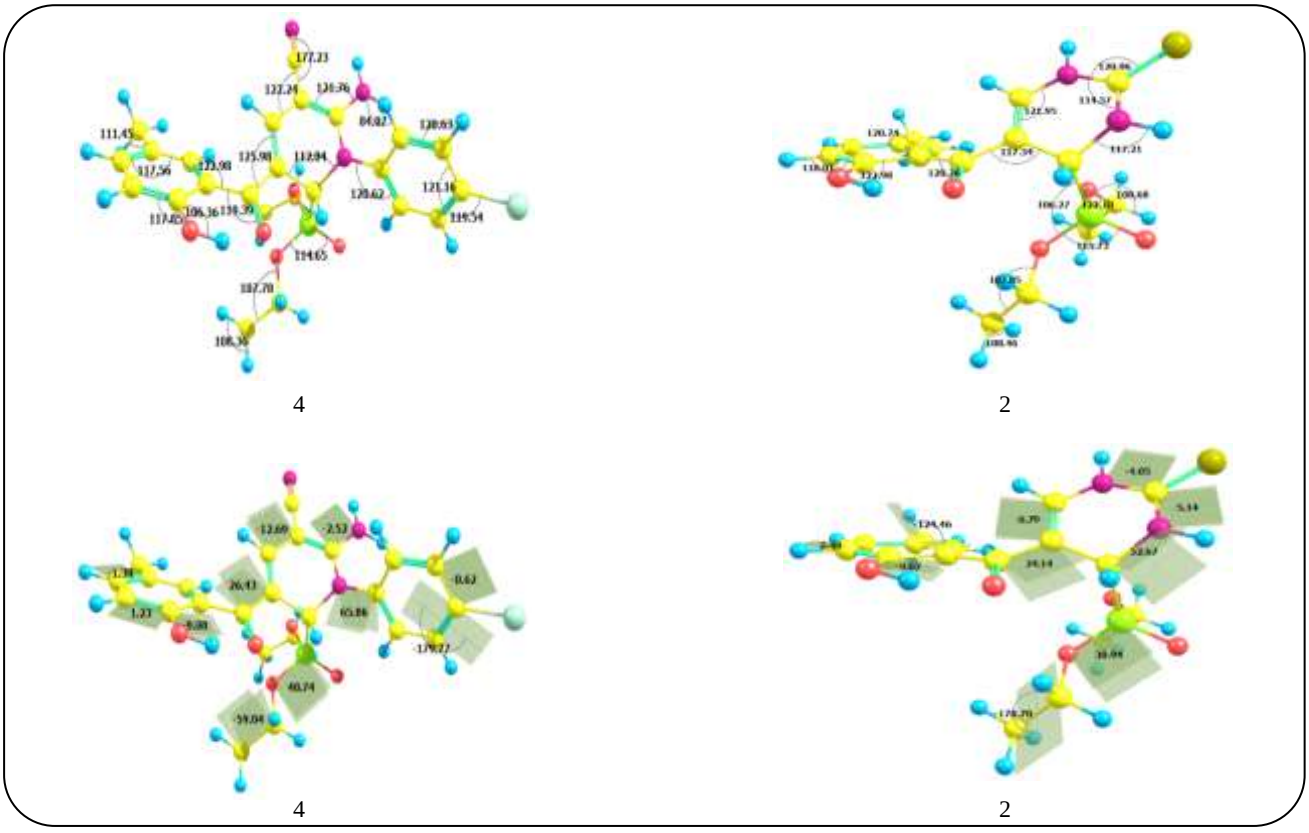

Fig. 10: Bond angle and dihedral angle of compounds 2 and 4 using B3LYP/6-311++G(d,p).

NBO Analysis

The second-order interaction energies between the donor and acceptor orbits Table 2 measures electronic offshoring in the systems studied. The higher the value of the interaction energy, the more intense the interaction between the donor and the acceptor. Also, a greater value of the interaction energy E^2 leads to greater stabilization of the molecular structure by this interaction. Analysis of the second-order perturbation theory of the Fock matrix shows strong intermolecular hyper-conjugative interactions formed by an orbital overlap. The results of NBO analysis of compounds **2** and **4** tabulated in Table 2 indicate that there is a strong hyper conjugative interactions LP (1) N_{26} → π*C_{18}- C_{19}, and π*C_4-C_5 → π*C_1-C_6, for **2** is 38.00, and 217.24 kcal/mol, respectively, and LP (1) O_{14} → π*C_4- C_5, and π*C_4-C_5 → π*C_1-C_6, for **4** is 36.50, and 250.84 kcal/mol, respectively. The C–N π orbital and amino group interact equally well with the pyridinyl ring. In fact, its interaction with the pyrimidinyl phosphonates ring is greater. Furthermore, the lone pair orbital of the nitrogen atom enjoys hyperconjugation with the C8–O9, and C1–C2 π* orbital. The oxygen and sulfur lone pair orbitals, on the other hand, interact essentially with the C23–N26 and C23–N24 π orbital of the pyrimidinyl phosphonates ring. It is surprising to notice a decrease in the population of the NBO P29–O30, C23–S27, P25–O26, C8–O9, and C4–C5 reflecting a charge transfer away from the pyridinyl and pyrimidinyl phosphonates ring. In conclusion, **2** and **4** enjoy the linear conjugation that is responsible for the observed spectrum.

Natural Charge

The distribution of electrons in various sub-shells of their atomic orbital is described by the analysis of the natural population [33] performed on the electronic structures of compounds **2** and **4**. The individual atom charges are presented in Tables 3 and 4. In the case of our studied compounds **2** and **4**, the most negative centers are O9, O14, N26, S27, N28, O30, O45, O46-atoms, and O9, O14, N24, O26, O41, O42, N56, N57-atoms, respectively. According to an electrostatic point of view of the molecule, these negative atoms tend to donate an electron. Whereas the most electropositive atoms such as; P29 and P25, Cl53-atoms respectively tend to accept an electron.

2	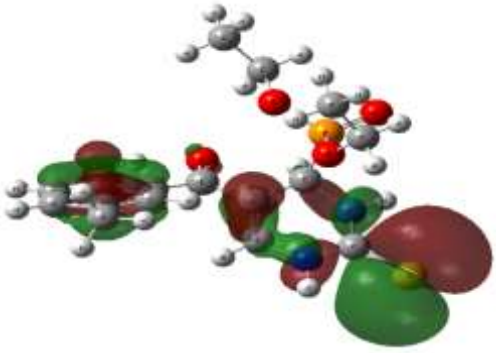	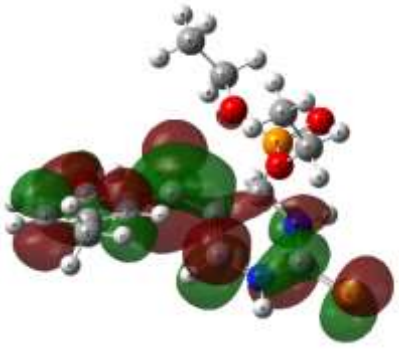
	HOMO	LUMO
4		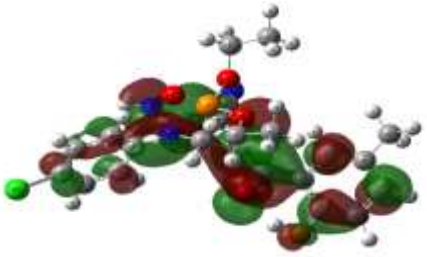
	HOMO	LUMO
ESP	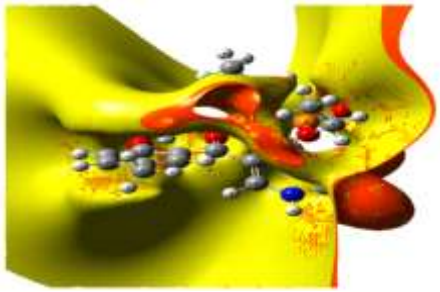	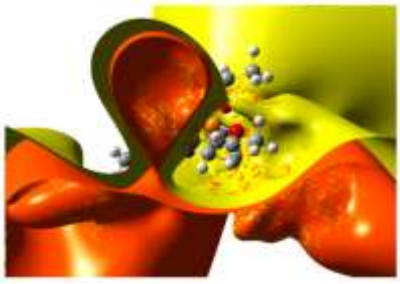
	2	**4**
3D-MEP	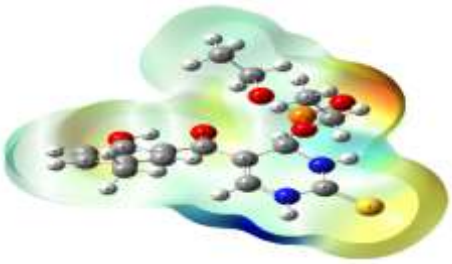	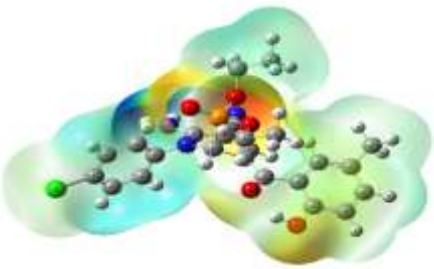
	2	**4**

Fig. 11: HOMO, LUMO maps, energy gap, ESP, and 3D-MEP for the studied compounds 2 and 4 using B3LYP/6-311++G(d,p).

Table 1: The Optimized calculations of total energies (a.u.), Zero point vibrational energies (kcal.mol^{-1}), Rotational constants (GHz), Entropies (cal.k^{-1}), energy of HOMO and LUMO (eV), energy gap (eV) , total dipole moment (Debye), the ionization potential (I /eV), electron affinity (A /eV), chemical hardness (η / eV), global softness (S/ eV^{-1}), chemical potential (V/eV^{-1}), electronegativity (χ /eV), and global electrophilicity index, (ω/eV), for compounds 2 and 4 at the B3LYP/6-311++G(d,p).

Parameters	(**2**)	(**4**)
Total Energy, (E_T)	-2272.03052	-1847.95153
Zero Point Vibrational Energy	185.07287	186.67287
Rotational constant	0.40608	0.61608
	0.06779	0.05449
	0.06297	0.05267
Entropy		
Total	170.720	171.820
Translational	43.813	44.713
Rotational	36.471	37.571
Vibrational	90.436	91.336
Energy of highest occupied molecular orbital (E_{HOMO})	-5.765312	-6.261984
Energy of lowest unoccupied molecular orbital (E_{LUMO})	-2.160224	-2.431408
Energy Gap, (E_g)	3.605088	3.830576
Dipole moment, (μ)	2.4559	5.7571
I (eV)	5.765312	6.261984
A(eV)	2.160224	2.431408
X(eV)	3.962768	4.346696
V(eV^{-1})	-3.962768	-4.346696
η(eV)	1.802544	1.915288
S(eV^{-1})	0.277386	0.261057
ω (eV)	1.099215	1.134737

Table 2: Second Order Perturbation Interaction Energy Values Computed in the NBO Basis for the studied compounds 2 and 4, calculated at B3LYP/6-311++G (d, p).

Compound	Donor	Acceptor	$E^{(2)a}$(kcal/mol)	NBO	Population
2	πC1-C6	π*C4-C5	23.28	C1-C6	1.70450
	πC4-C5	π*C8-O9	25.18	C4-C5	1.60003
	LP(1) O9	RY*C8	10.88	LP(1) O9	1.96905
	LP(2) O9	π*O14-H15	15.11	LP(2) O9	1.88046
	LP(2) O14	π*C4-C5	37.30	LP(2) O14	1.81929
	LP (1) N26	π*C18-C19	38.00	LP (1) N26	1.64306
	LP (1) N26	σ*C23-S27	20.09	LP (2) S27	1.88302
	LP (2) S27	σ*C23-N26	12.32	LP(2) O46	1.80604
	LP(2) O46	σ*C20-P29	18.37	LP(3) O46	1.78886
	LP (3)O46	σ*P29-O30	22.79	C4-C5	0.43454
	π*C4-C5	π*C1-C6	217.24	π*C23-S27	0.30632
	π*C8-O9	π*C4-C5	80.36	σ*P29-O30	0.16614
	σ*C23-S27	σ*C23-S27	151.36	σ*P29-O45	0.18087
	σ*P29-O30	σ*O30-C32	38.59		
	σ*P29-O45	RY*P29	11.87		
4	πC4-C5	π*C8-O9	24.78	C4-C5	1.60312
	πC23-C54	π*C18-C19	24.13	C23-C54	1.68795
	πC23-C54	π*C55-N56	24.68	LP(1) O9	1.96803
	LP(1) O9	RY*C8	10.49	LP(2) O9	1.88289
	LP(2) O9	π*O14-H15	15.64	LP(2) O14	1.82349
	LP(2) O14	π*C4-C5	36.50	LP (1) N57	1.73596
	LP (1) N57	π*C23-C54	52.92	LP(3) O42	1.79812
	LP (3)O42	σ*P25-O26	21.39	LP(2) O42	1.81266
	LP(2) O42	σ*C20-P25	17.82	LP (3)Cl53	1.92388
	LP (3)Cl53	π*C46-C50	12.74	LP (1) N56	1.96856
	LP (1) N56	RY*C55	16.60	C4-C5	0.43172
	π*C4-C5	π*C1-C6	250.84	C8-O9	0.31248
	π*C8-O9	π*C4-C5	76.48	C23-C54	0.46102
	π*C23-C54	π*C55-N56	17.18	P25-O26	0.16074
	σ*P25-O26	σ*O26-C28	43.34	P25-O41	0.17540
	σ*P25-O41	RY*P25	11.05		

[a] *$E^{(2)}$ means the energy of hyperconjugation interactions (stabilization energy).*

$LP_{(n)}$ is a valence lone pair orbital (n) on the atom.

Table 3: Natural Charge, Natural Population, and Natural electronic Configuration of active sites studied compounds 2 and 4 using B3LYP/6-311++G (d,p).

Compound	Atom No.	Natural Charge	Natural Population				Natural electronic Configuration
			Core	Valence	Rydberg	total	
2	O9	-0.65309	1.999	6.644	0.0088	8.653	[core]2S(1.70)2p(4.95)
2	O14	-0.66668	1.999	6.658	0.0086	8.667	[core]2S(1.65)2p(5.01)
2	N26	-0.58452	1.999	5.570	0.0156	7.584	[core]2S(1.24)2p(4.33)3p(0.01)
2	S27	-0.21050	9.999	6.180	0.0317	16.21	[core]3S(1.76)3p(4.41)4S(0.01)3d(0.01)
2	N28	-0.60045	1.999	5.582	0.0188	7.600	[core]2S(1.24)2p(4.34)3p(0.01)
2	P29	2.31896	9.998	2.550	0.1330	12.68	[core]3S(0.80)3p(1.75)3d(0.10)4p(0.02)
2	O30	-0.85024	1.999	6.840	0.0101	8.850	[core]2S(1.68)2p(5.16)
2	O45	-0.85237	1.999	6.842	0.0103	8.852	[core]2S(1.69)2p(5.15)3p(0.01)
2	O46	-1.06845	1.999	7.062	0.0067	9.068	[core]2S(1.81)2p(5.25)
4	O9	-0.67471	1.999	6.666	0.0086	8.675	[core]2S(1.70)2p(4.97)
4	O14	-0.67249	1.999	6.664	0.0086	8.672	[core]2S(1.65)2p(5.02)
4	N24	-0.46210	1.999	5.446	0.0171	7.462	[core]2S(1.16)2p(4.29)3p(0.01)
4	P25	2.33194	9.998	2.539	0.1307	12.67	[core]3S(0.80)3p(1.74)3d(0.10)4p(0.02)
4	O26	-0.84668	1.999	6.837	0.0102	8.847	[core]2S(1.68)2p(5.16)
4	O41	-0.85381	1.999	6.844	0.0103	8.854	[core]2S(1.69)2p(5.16)3p(0.01)
4	O42	-1.08939	1.999	7.083	0.0065	9.089	[core]2S(1.81)2p(5.27)
4	Cl53	0.00154	9.999	6.979	0.0193	16.99	[core]3S(1.83)3p(5.15)3d(0.01)4p(0.01)
4	N56	-0.36178	1.999	5.342	0.0199	7.362	[core]2S(1.58)2p(3.76)3d(0.01)
4	N57	-0.75212	1.999	5.744	0.0088	7.752	[core]2S(1.29)2p(4.46)3p(0.01)

Table 4: Natural population of the total electrons in studied compounds 2 and 4 using B3LYP/6-311++G (d,p).

Parameters	**2**	**4**
Core	65.97936 (99.969% of 66)	83.97025 (99.965% of 84)
Valence Lewis	131.91745 (96.998% of 136)	172.37212 (96.838% of 178)
Total Lewis	197.89681 (97.969% of 202)	256.34237 (97.841% of 262)
Valence non-Lewis	3.60444 (1.784% of 202)	5.06067 (1.932% of 262)
Rydberg non-Lewis	0.49876 (0.247% of 202)	0.59696 (0.228% of 262)
Total non-Lewis	4.10319 (2.031% of 202)	5.65763 (2.159% of 262)

For the numbering system, see Fig. 9

Nonlinear optical (NLO) Analysis

In the literature no study around NLO experimentally or theoretically for the studied molecules, therefore, this Attention to this study. Non-linear optical properties are the ability of any compound to convert light of a longer wavelength into light of a shorter wavelength. Most applications of single crystals of any nonlinear materials are evident in the fields of semiconductors, infrared detectors, solid-state lasers, photosensitive materials, and crystalline thin films for microelectronics [34]. NLO parameters and the electronic structure relationship were investigated theoretically by using DFT/B3LYP/6-311++G (d,p) of the studied compounds **2** and **4**. Total static dipole moment (μ), the mean polarizability, α,

Table 5: Total static dipole moment (μ), the mean polarizability (<α>), the anisotropy of the polarizability (Δα), and the mean first-order hyperpolarizability (<β>), for studied compounds 2 and 4 by B3LYP/6-311++G (d,p).

Property	PNA	2	4
μ_x		-4.3187Debye	0.9179Debye
μ_y		0.5317Debye	2.0967Debye
μ_z		3.7696Debye	-0.8905Debye
μ	2.44 Debye [a]	5.7570Debye	2.4559Debye
α_{XX}		-181.8339a.u.	-202.3811 a.u.
α_{XY}		11.7509a.u.	-1.6349 a.u.
α_{YY}		-160.8346a.u.	-215.0525 a.u.
α_{ZZ}		-156.2737a.u.	-226.9397 a.u.
α_{YZ}		-3.7693a.u.	-9.9104 a.u.
α_{XZ}		-2.2505a.u.	12.3524 a.u.
< α>	22×10^{-24} cm^3 [b]	34.52×10^{-24} esu	44.12×10^{-24} esu
Δα		45.13×10^{-24} esu	55.20×10^{-24} esu
βxxx		-128.8290a.u.	-123.7811a.u.
βxxy		35.8124a.u.	22.4723a.u.
βxyy		-53.6827a.u.	11.6665a.u.
βyyy		68.9299a.u.	91.0158a.u.
βxxz		61.9792a.u.	51.3682a.u
βxyz		15.4675a.u.	24.8137a.u.
βyyz		10.0424a.u.	-3.3070a.u.
βxzz		29.1339a.u.	44.9678a.u.
βyzz		18.5023a.u.	-43.4167a.u.
βzzz		19.8387a.u.	-197.2227 a.u.
< β>	15.5×10^{-30} esu [c]	24.61×10^{-30} esu	35.82×10^{-30} esu

a, b, c) PNA results are taken from references [35–37].

the anisotropy of the polarizability Δα, the mean first-order hyperpolarizability, (β) of the studied compounds **2** and **4** are listed in Table 5. No experimental values of NLO properties of the studied compounds so; P-nitro aniline (PNA) was chosen as a reference. The values of, α, β in Table 5 show that the order of increasing α with respect to PNA is: compounds **2** and **4** are ~ 1.5 and 2 times higher than (PNA), respectively. The analysis of the β parameter shows that compounds **2** and **4** are ~ 2 and 2.5 times higher than (PNA), respectively [35-37]. Therefore, the studied compounds show promising optical properties.

Molecular Electrostatic Potential (MEP)

The chemical reactivity of a molecule can be determined from Molecular Electrostatic Potential (MEP), which simultaneously displays molecular shape, size, and electrostatic potential in terms of color gradation. The electrostatic potential generated in the space around a molecule by the charge distribution is useful for understanding the electrophilic or nucleophilic properties [38]. DFT/B3LYP/6-311++G (d,p) method of calculation of studied compounds **2** and **4** are calculated 3D MEP and ESP from the optimized molecular structure are shown in Figs. (11-13). Potential increases in the order following: red < orange < yellow < green < blue [39, 40]. The results show that the negative region (red) is mainly over the N, P, and O atomic sites, which is caused by the contribution of lone-pair electrons of nitrogen and oxygen atoms while the positive (blue) potential sites are around the hydrogen, sulfur, carbon, and Cl atoms. A portion of the molecule that has negative electrostatic potential will be susceptible to electrophilic attack—the more negative the higher the tendency for the electrophilic attack.

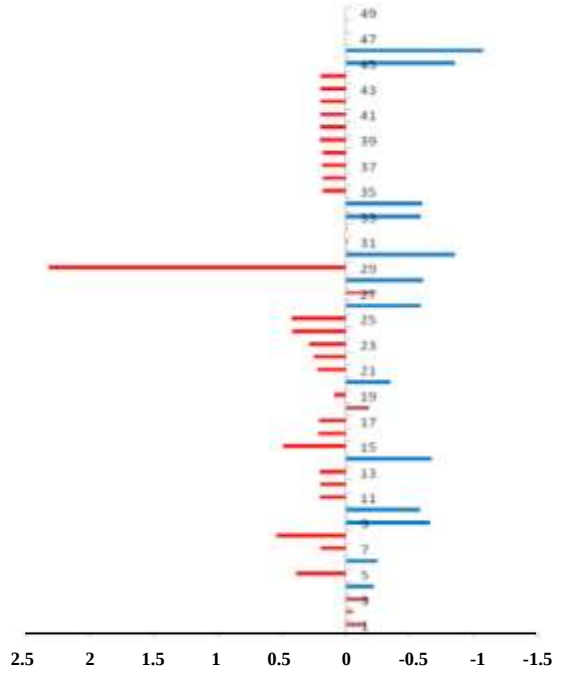

Atomic charge distribution

Fig. 12: Atomic charge distribution (e) for compound 2 using B3LYP/6-311++G (d,p).

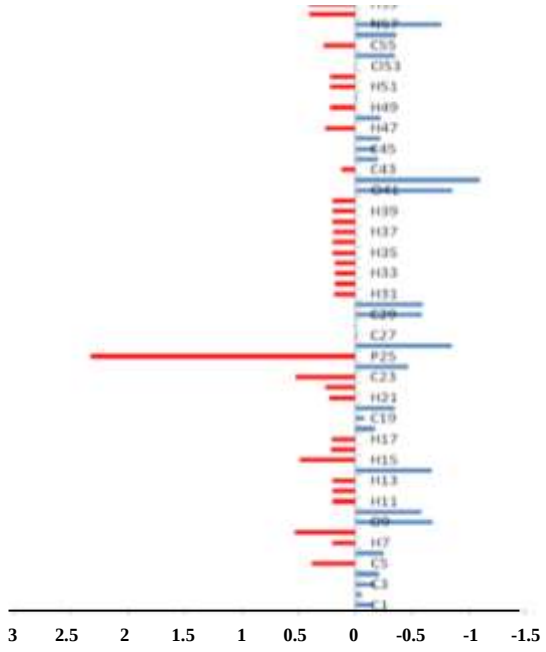

Atomic charge distribution

Fig. 13: Atomic charge distribution (e) for compound 4 using B3LYP/6-311++G (d,p).

NMR analysis

DFT theory in the gas and DMSO solvent was calculated ^{1}H and ^{13}C chemical shifts of the title molecules with the experimental NMR in DMSO solvent is gathered in Figs 3-6. Primarily, the full geometry optimization of the molecules was performed at the gradient-corrected DFT using the hybrid B3LYP method and GIAO [41-43]. ^{1}H and ^{13}C chemical shift calculations of the compounds were made by the same method using a 6–311++G (d,p) basis set in gas and DMSO solvent. From the computed and experimental chemical shift values, H6, H7, H8 & H9 attached to the carbon atoms of the benzene ring have smaller values than the other proton (H28) and carboxyl proton (H32) signals due to the electronic charge density around the ring. In the experimental ^{13}C NMR spectrum (DMSO), the value of δ (chemical shift) of carbon atoms is absorbed between 16-183 ppm. The molecule has ten carbons however these carbons are differentiated into three groups (attached with benzene, pyrimidine, carboxyl) which is consistent with the structure and molecular symmetry.

Vibration assignments of compounds 2 and 4

Comparison of the vibration frequencies calculated at DFT/B3LYP/6-311++G (d,p) with experimental values (c.f. Table 6) and corresponding assignments of FT-IR Spectra of compounds **2** and **4** are listed in Figs. (1-2). Another attempt to follow up with the changes in the studied compounds **2** and **4** is carried out by studying vibration spectra. The occurrence of any contradiction between the calculated and the experimental vibration frequencies can be because the calculations were implemented onto a single molecule (i.e., gaseous state). The Assignment could be achieved extensively as in the following:

The Computed vibration is assigned to be, OH, N–H twisting vibration at 3480, 3578 cm^{-1} for compounds **2** and **4** which has shown a comparable agreement with experimental results at 3293, 3297 cm^{-1}. The aromatic C–H stretching vibrations [44] is in general observed in the region 3000–3100 cm^{-1}. The Computed vibration is assigned to C–H aromatic stretching vibrations at 3271 cm^{-1} for compounds **2** and **4** which is comparable with experimental results at 3050 cm^{-1}. The Computed vibration is assigned to symmetric C–H aliphatic stretching vibration in CH_3 at 2995, 2950, 2990, 2890 cm^{-1} for compounds **2** and **4** has shown a comparable agreement with experimental results at 2980, 2927, 2983, 2917 cm^{-1}. The Computed vibration is assigned to asymmetric C≡N

Table 6: Experimental and computational calculated vibrational wave- numbers (harmonic frequency (cm^{-1})), IR intensities and assignments for studied compounds 2 and 4 by B3LYP/6-311++G (d,p).

No.	$\upsilon_{exp.}(cm^{-1})$		$\upsilon_{the.}(cm^{-1})$		Intensity		Assignment
	2	4	2	4	2	4	
1	3293	3297	3480	3578	56.98	66.89	br, OH, NH twisting
2	3050	3050	3271	3271	230.16	210.61	$C–H_{arom}$, Sym Stretching
3	2980, 2927	2983, 2917	2995, 2950	2990, 2890	220.66	217.16	$C–H_{aliph}$, Asym Stretching
4	----------	2228	---------	2325	115.9	120.9	C≡N, Asym
5	1641	1638	1665	1650	96.57	86.57	C=O , Sym Stretching
6	1619	1593	1625	1630	31.47	51.47	C=C (in ring)
7	1214	1225	1200	1220	105.25	112.25	P=O, Asym
8	1044	1025	1010	1060	25.68	45.68	P–O–C, bending
9	1165	---------	1175	------	123.02	132.02	C=S, Sym

Asym-stretching vibration at 2325 cm^{-1} for compound **4** has shown a comparable agreement with experimental results at 2228 cm^{-1}. Generally, the C=O vibrations [44] are observed in the region 1790-1810 cm ^{1}. Vibrations are assigned to C=O stretching at 1665, 1650 cm^{-1} for compounds **2** and **4** which is comparable with experimental results at 1641, 1638 cm^{-1} respectively. The C=C vibrations [45] are in general observed in the region 1480-1630 cm ^{1}. The Computed vibration is assigned to C=C stretching vibrations at 1625, 1630 cm^{-1} for compounds **2** and **4** which is comparable with experimental results at 1619, 1593 cm^{-1}. The Computed vibration is assigned to P=O stretching vibrations at 1200, 1220 cm^{-1} for compounds **2** and **4** which is comparable with experimental results at 1214, 1225 cm^{-1}. Vibrations are assigned to P-O-C binding stretching at 1010, 1060 cm^{-1} for compounds **2** and **4** which is comparable with experimental results at 1044, 1025 cm^{-1} respectively. The Computed vibration is assigned to symmetric C=S stretching vibration at 1175 cm^{-1} for compound **2** and has shown a comparable agreement with experimental results at 1165 cm^{-1}.

Table 1 shows the Zero-Point Vibrational Energies (ZPVE), calculated thermal several parameters, and the entropy, S_{Vib} (T). The total energies and the change in the total entropy of compounds **2** and **4** at room temperature using B3LYP/6-311++G (d,p) are also presented. The most important orbital in a molecule is the frontier molecular orbital (highest occupied molecular orbital, HOMO, and lowest unoccupied molecular orbital, LUMO).

TD-DFT Study of the Absorption Spectrum of studied compounds 2 and 4

Using the TD-DFT method, we determined the theoretical absorption spectra of studied compounds **2** and **4** from the ground state of each molecule. These theoretical absorption spectra are calculated in a vacuum at level B3LYP / 6-311++G (d, p). Tables 7 and 8 compare the wavelengths (λ) and the oscillator force (f) corresponding to the maximum absorption for compounds **2** and **4** . Figures 14 and 15 show that the dimerization, therefore, has a hyperchromic effect on the absorption bands of compounds **2** and **4** studied. Figs. 14-15 and Tables 7-8 present the experimental and theoretical electronic absorption spectra of **2** and **4** in dioxane and methanol. The spectrum of **2** and **4** is composed of four bands in the range of 200–450 nm. The spectrum in dioxane shows four intense bands at 338 nm, 299, 279, and 215 nm for compound **2**, also: at 375 nm, 240 nm, 225 nm, and 215 nm for compound **4.** Increasing solvent polarity ongoing from dioxane to methanol results in a blue shift. The four observed bands are assigned as (π–π*) transitions, as indicated by the values of molar absorptive (ε =35000), and (ε = 45000). These results in an increase in the absorption intensity of these compounds **2** and **4** studied compared to that of the pyrimidinyl phosphonates nucleus. There is also a displacement of the absorption bands towards the visible. This increase in wavelengths reflects a bath chromic effect due to dimerization. The pyrimidinyl phosphonates ring of compounds **2** and **4** studied absorb in the ultraviolet and visible fields. The analysis in Tables 7 and 8 indicates that the absorption

Table 7: Theoretical and experimental UV spectra of compound 2 calculated at CAM-B3LYP/6–311++G (d, p).

TD-Theoretical													Experimental	
Gas phase					Dioxane				methanol				methanol Dioxane	
state	Config uration	Coefficient	f	λ, nm	Config uration	Coefficient	f	λ, nm	Configuration	Coefficient	f	λ nm	$\lambda_{,nm}$	$\lambda_{,nm}$
I	98 -102 99 -103 100 -102 101 -102	0.154 -0.137 -0.375 0.531	0.320	325	98 -102 100 -102 100 -103 101 -102	0.163 0.114 -0.180 0.625	0.410	330	98 -102 100-102 100-103 101-102 101-103	0.155 0.165 -0.130 0.632 0.125	0.400	328	332	338
II	98 -102 99 -102 100 -102 101 -103	0.471 0.383 0.231 0.181-	0.147	294	98 -102 99 -102 100 -102 101 -102 101 -103	0.420 0.259 0.404 -0.131 -0.213	0.155	295	98 -102 99 -102 100-102 101-102 101-103	0.361 0.214 0.456 -0.190 -0.210	0.111	295	297	299
III	96 -102 98 -102 98 -103 99 -102 99 -103 100 -102 101 -102	0.137 0.416 0.173- 0.384- 0.161 -0.131 -0.245	0.127	273	96 -102 98 -102 98 -103 99 -102 99 -103 100 -102 100 -103	0.121 0.457 0.199- 0.250- 0.121 -0.326 0.166	0.191	271	98 -102 98 -103 99 -102 100-102 100-103	0.503 -0.246 0.139- 0.331- 0.151	0.263	270	275	279
IV	97 -102 97 -103 97 -105 99 -104 100 -104 100 -105 101 -104 101 -105	0.207 0.286- 0.114 0.220- 0.311- 0.114 0.380 -0.132	0.189	205	97 -102 97 -103 97 -105 100 -104 101 -104 101 -105	0.183- 0.248 0.102- 0.178- 0.515 0.220	0.256	207	97 -102 97 -103 97 -105 100-104 101-103 101-104 101-105	-0.192 0.265 0.111- 0.122- 0.109- 0.511 0.245	0.214	206	210	215

the spectrum of studied compounds **2** and **4** have ionizing radiation between 200 and 400 nm. The compounds **2** and **4** studied have four absorption bands in their UV spectrum. For compound **2**, The experimental band at 338 nm (in dioxane) is reproduced theoretically by using PCM (dioxane), at 330 (state I) nm, and in the gas phase at 325 nm as shown in Table 7. Single-point energy (a state I), theoretical excitations band reproduce at 328 nm in methanol indicating that the calculated wavelength is lower than the observed wavelength. The experimental second band observed at 299 nm in dioxane, is reproduced theoretically at 295 nm (state II). The gas-phase calculation gives a wavelength of 294 nm. Moreover, in methanol, this same band appears at 297 nm, whereas theoretical calculations in methanol reproduce this band at 295 nm (state II), as shown in Table 7. The third $(\pi\text{-}\pi^*)^1$ state experimentally at 279 nm in dioxane, is reproduced theoretically at 271 nm (state II), which involves the orbital's φ_{98} and $\varphi_{102,}$ in the transition. The wavelength at 273 nm in gas-phase calculation gives (state III), at the same orbitals. In methanol, this same band appears theoretically at 270 nm, (state III), as shown in Table 7. The 215 nm experimental in dioxane, four-band is reproduced theoretically at 207 nm (stage IV). The gas-phase calculation gives a wavelength of 205 nm. Moreover, in methanol, this same band appears at 210 nm, whereas theoretical calculations in methanol reproduce this band at 206 nm (state IV), as shown in Table 7. The five orbitals" φ_{98}, φ_{100}, φ_{101}, $\varphi_{102,}$ and φ_{104} respectively, involved in the theoretical transitions of **2**, are shown in Fig. 16, where the first, second, third, and fourth bands involving $\varphi_{100,}$ φ_{101}, φ_{98} & $\varphi_{102,}$ and φ_{104} show a delocalization of electron density, and Charge Transfer CT character. For compound **4**, State (I) the non-polar solvent (dioxane), shows the spectrum band experimentally at 375 nm is reproduced theoretically at 367 nm (a state I), as shown in Table 8, which involves orbital's φ_{131} and φ_{132}. The gas phase computed theoretically gives a vertical excitation at 365 nm (a state I). A blue shift of λ_{max} due to increasing solvent polarity of this band to 370 nm. The polar solvent (methanol) appeared theoretically band at 366 nm (a state I). The state II at 240 nm experimentally in dioxane is reproduced theoretically at 235 nm, this transition indicates that the orbital's φ_{129} and φ_{132}. Theoretical gas-phase calculations give a wavelength of 234 nm (state II),

Table 8: Theoretical and experimental UV spectra of compound 4 calculated at CAM-B3LYP/6–311++G (d, p).

TD-Theoretical													Experimental	
Gas phase					Dioxane				methanol				methanol Dioxane	
state	Config uration	Coefficient	f	λ, nm	Config uration	Coefficient	f	λ, nm	Configuration	Coefficient	f	λ, nm	$\lambda_{,nm}$	$\lambda_{,nm}$
I	131-132 131-135	0.674 0.117	0.395	365	131-132 131-135	0.674 -0.114	0.489	367	131-132 131-135	0.675 0.116	0.4 15	366	370	375
II	127 -132 128 -132 128 -133 130 -132 130 -133 130 -135 130 -137 131 -132	0.123 0.381 0.109 0.145 -0.328 0.345 -0.125 0.117	0.113	234	125 -132 127 -132 127 -133 129 -132 129 -133 129 -134 131 -134	0.147 -0.114 0.131 0.467 -0.292 0.200 -0.225	0.133	235	125-132 127-132 127-133 129-132 129-133 129-134 131-134	0.149 0.115- 0.232 0.367 -0.291 0.280 -0.165	0.2 11	234	237	240
III	129 -133 129 -135 130 -136 131 -136 131-137 131 -138 131 -140 131-141 131 -142	0.273- 0.163- 0.116- 0.315 -0.300 0.117 -0.126 0.223 0.168	0.241	215	129 -133 129 -135 130 -136 131 -136 131-137 131 -140 131 -141	0.219- 0.142 0.129- 0.367 -0.318 -0.264 0.113	0.344	217	129-133 129-135 130-136 131-136 131-137 131-140 131-141	0.289- 0.152 0.119- 0.327 -0.308 -0.164 0.213	0.3 51	218	220	225
IV	128 -132 128 -133 128 -135 130 -133 130-136 130 -137 131 -136 131 -137	0.228 0.147- 0.204 0.200 0.290 0.317 0.250 0.181	0.152	207	128 -132 128 -133 128 -135 130 -133 130-136 130 -137 131 -136 131 -137	0.195 0.133- 0.173- 0.175 0.307 0.384 0.234 0.211	0.261	208	128-132 128-133 128-135 130-133 130-136 130-137 131-136 131-137	0.228 0.147- 0.204 0.200 0.290 0.317 0.250 0.181	0.2 52	207	210	215

in methanol, observed at 237 nm, and reproduce theoretically at 234 nm, which is lower than the observed wavelength, where the transition orbitals are φ_{129} and φ_{132}. The state III third band in dioxane at 225 nm, experimentally, and at 217 nm theoretically, indicates that the orbital's φ_{131} and φ_{136} are involved in this transition. 215 nm theoretical gas-phase, and in methanol at 218 nm (state III), where the orbital's φ_{131} and φ_{136} are involved in this transition. The four-band observed experimentally in dioxane at 215 nm, is reproduced theoretically at 208 nm (stage IV), indicating that the orbital's φ_{130} and φ_{137} are involved in this transition. Theoretical gas-phase calculations give a wavelength of 207 nm (stage IV). This same band is observed at 210 nm in methanol, whereas theoretical calculations in methanol reproduce this band at 207 nm (stage IV). The seven orbitals' φ_{128}, φ_{129}, φ_{130}, φ_{131}, φ_{132}, φ_{136}, and φ_{137} involved in the theoretical transitions of **4**, are shown in Fig. 16. The first band which involves φ_{129} and φ_{130} has electron density delocalization, while orbital's φ_{128}, φ_{131}, φ_{132}, φ_{136}, and φ_{137} have a Charge Transfer CT character.

Antimicrobial activity

Biological activities of synthesized compounds **2** and **4** were studied for antibacterial and antifungal properties against different types of bacteria; Gram-positive- *S. aureus,* and *B. subtilis* and Gram-negative- *S. Typhimurium* and *E. Coli* also*; Yeast -C. albicans* for fungus. *A. fumigatus.* Measuring recorded results of the growth inhibition (zone of inhibition) surrounding the disc of the material. Results showed in Table 9 and Fig. 17. Some antibiotics were evaluated for their antibacterial activities and their results were found ineffective for all bacteria and fungi. Compounds **2** and **4** give more explanation of the high antimicrobial activity against all tested bacteria and fungi in which the small size of compound **4** increases its absorption ability on the surface of the cell wall of microorganisms and the respiration process of the cell. Hence, compound **4** is essential for the growth-inhibitor effect.

Structure-Activity Relationship (SAR)

The biological activity of the prepared compounds **2** and **4** can be correlated to the calculated ground state energetic and global properties. From (Table 1 and 9); The biological activity of the studied compound (**2** and **4**) obtained experimentally follow the order **4** > **2**, Against

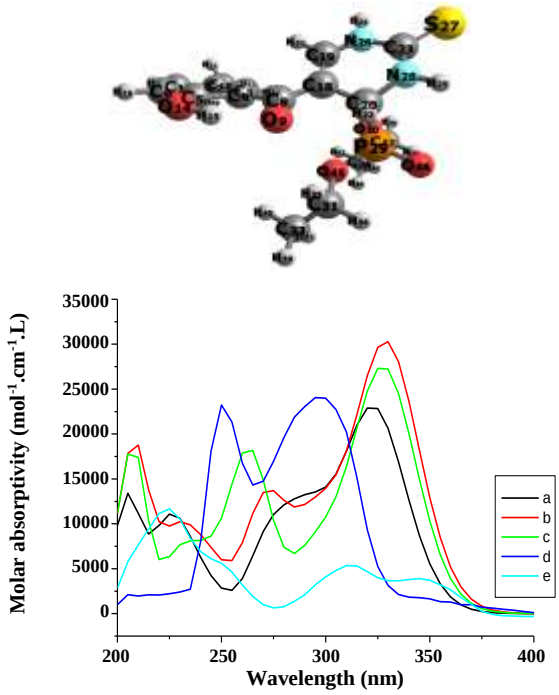

Fig. 14: Electronic absorption spectra of compound 2 (a) theoretical in the gas phase, (b) theoretical in dioxane, (c) theoretical in methanol, (d) experimental in dioxane, (e) experimental in methanol.

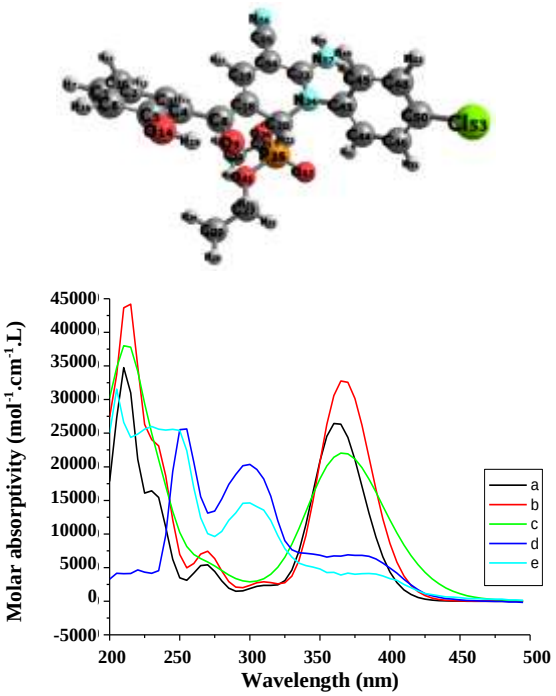

Fig. 15: Electronic absorption spectra of compound 4 (a) theoretical in the gas phase, (b) theoretical in dioxane, (c) theoretical in methanol, (d) experimental in dioxane, (e) experimental in methanol.

G+, G-, and fungi. Theoretically, the chemical reactivity can be explained in terms of the energy gap, Eg, of the studied compound computed at B3LYP/6-311++G (d,p) following the same order obtained experimentally indicating that Eg is one factor contributing to the reactivity of the studied compounds, E_{HOMO} which measures the donating power, the order of E_{HOMO} **4 > 2**, and dipole moment which measure the charge separation, the order of the dipole moment **2 > 4**, (c.f. Table 1). The theoretically computed global softness (S), global electrophilicity index, (ω), electronegativity (χ), and chemical potential (V) of the studied compounds follow the same order of the experimental biological activity which is **4 > 2**. Whereas the chemical hardness (η) follows the reverse order of the experimental biological activity **2 > 4.** In the case of natural charge from NBO and mean first-order hyperpolarizability (β), the order is **4>2** and **4>2** respectively, which violates the order of the experimental biological activity. In conclusion, the substituent in compounds **2** and **4** increases its biological activity**.**

Summary and Conclusion

To know the reactive behavior of synthesized compounds **2** and **4**, a study was carried out using (TD) DFT with the base game B3LYP/6-311++G (d, p). The molecules are soft (as the energy gap is less), considered as from HOMO & LUMO analysis, higher reactivity as an electrophilic (higher electrophilicity index), and more reactive (hardness is less), it is confirmed that global reactivity descriptors. The charges predicted by MEP were found supported by the chemical shift analysis from the NMR study. From NBO analysis, the most probable transitions in the molecules are identified. The vibrational wavenumbers computed theoretically were found to agree well with the experimental values. The excitation energies, maximum wavelengths, oscillator strength, and electronic transitions of each compound were determined using the TD-DFT method at level CAM-B3LYP/6-311++G (d, p) to reproduce the experimental spectra, indicating a good agreement between theory and experiment. These data allowed us to conclude that the absorption spectrum of compounds **2** and **4** is observed in the ultraviolet (200 - 400 nm). Electronic absorption spectra are investigated experimentally in a non-polar solvent (dioxane) and a polar solvent (methanol). The band maxima (λ_{max}) and intensities of the spectra are found to have solvent dependence. The bands of compounds **2** and **4** show a blue shift. The intramolecular

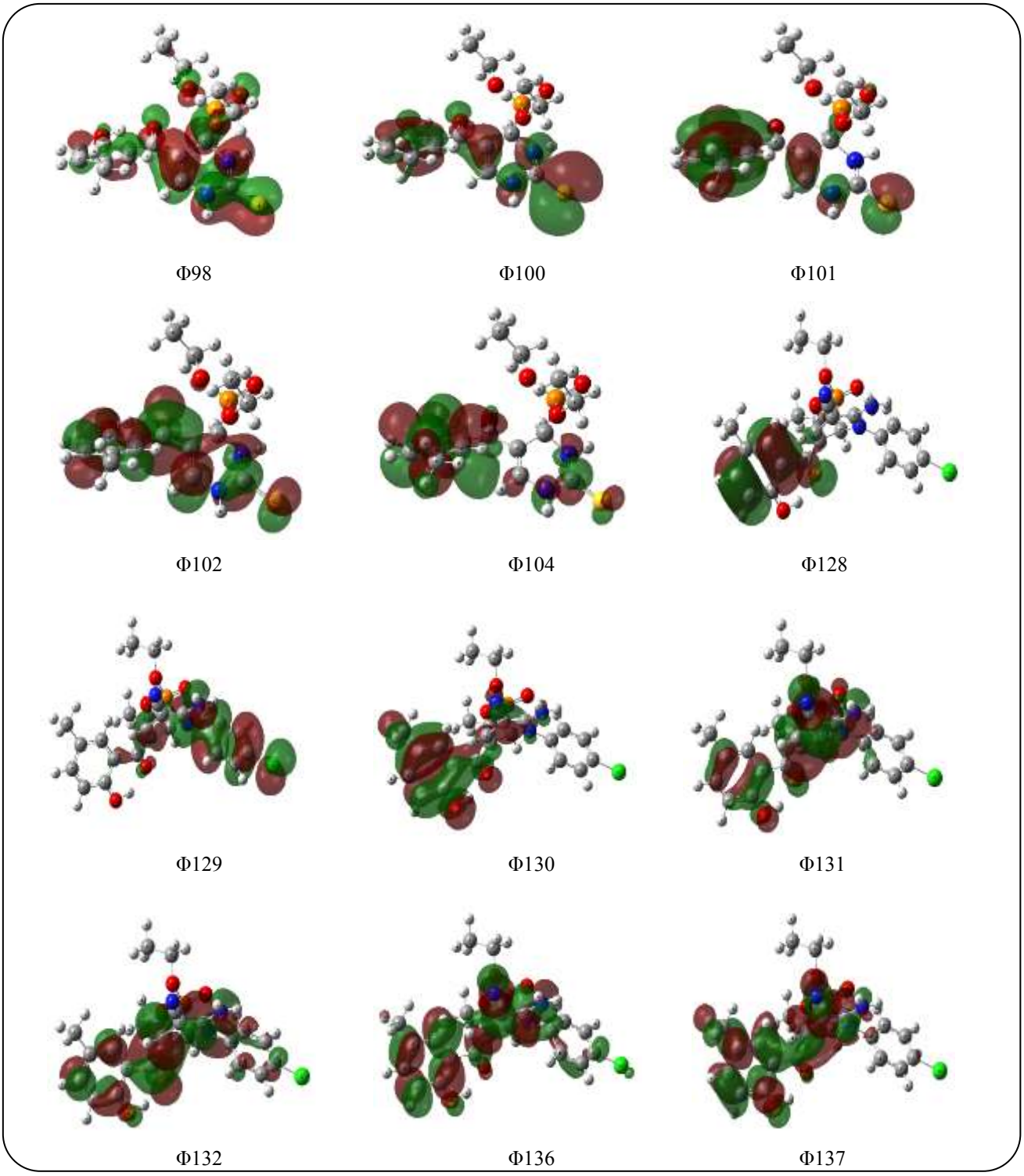

Fig. 16: Electron density contours of compounds 2 and 4.

electronic transitions which stabilize these compounds are LP (1) $N_{26} \rightarrow \pi^*C_{18}$- C_{19}, and π^*C_4-$C_5 \rightarrow \pi^*C_1$-C_6, for **2** is 38.00, and 217.24 kcal/mol, respectively, and LP (1) $O_{14} \rightarrow \pi^*C_4$- C_5, and π^*C_4-$C_5 \rightarrow \pi^*C_1$-C_6, for **4** is 36.50, and 250.84 kcal/mol, respectively, as stabilization energies. By studying the influence of the medium on compounds

Table 9: In vitro antimicrobial activities of the synthesized compounds at 500 and 1000 μg/mL and the MIC values for some selected compounds.

Compd.	Conc. (μg/mL)	Zone of inhibition in mm* and (MIC values in μg/mL)					
		Bacteria Gram (+) ve		Bacteria Gram (□) ve		Fungi	Yeast
		A. fumigatus	*C. albicans*	*E. coli*	*S. typhimurium*	*B. subtilis*	*S. aureus*
2	500	-	-	-	-	14 (250)	-
	1000	-	-	-	-	20	-
4	500	-	-	-	-	12	-
	1000	-	-	-	-	16	-
S**	500	26	25	28	27	28	26
	1000	35	35	36	38	35	37

** Low active: 6–12 mm; moderately active: 13–19 mm; highly active: 20–30 mm; –: No inhibition or inhibition less than 5 mm.*
S**: *Standard drugs*

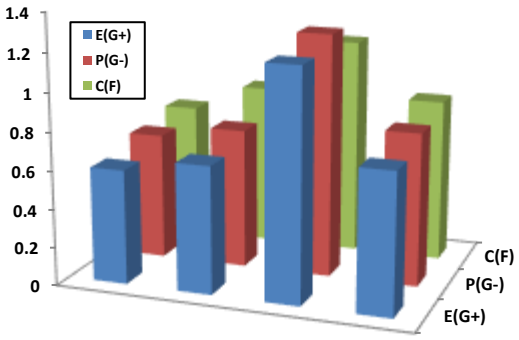

Fig. 17: Antimicrobial activity for the studied compounds 2 and 4 against gram-positive bacteria (G^+), gram-negative bacteria (G^-), and Fungi (F).

2 and **4**, it turns out that are more reactive and more soluble in polar solvents. Theoretically, the reactivity of the studied compounds follows the order: **4 > 2** which is the same order of reactivity towards G^-, G^+, and fungus. Finally, the purpose of this reported theory result is to prove the stability of the optimized structure for two compounds **2** and **4**. Also; we investigate theoretical analysis for an application used for these compounds such as optical properties, microorganisms, NBO analysis, etc.

Received: Mar. 3, 2021; Accepted: May 31, 2021

REFERENCES

[1] Sosnovskikh V. Ya., Irgashev R. A., Reactions of 3-(polyfluoroacyl)chromones with Indole and N-Methylindole, *Russian Chemical Bulletin*, **55**: 2294–2295 (2006).

[2] C. Ghosh K., Patra A., One-Pot Synthesis of Pyrano[3,4-b] Chromones from Chromone-3--Carbaldehyde, *J. Heterocycl. Chem.* **45**: 1529- 1543 (2008).

[3] V. Sosnovskikh Y., Moshkin V.S., Kodess M.I., Unsaturated Polyfluoroalkyl Ketones in the Synthesis of Nitrogen-Bearing Heterocycles, *Tetrahedron* **64:** 7877– 7889 (2008).

[4] A. Plaskon S., Grygorenko O.O., Ryabukhin S.V., Recyclization of 3 Formylchromones with Binucleophiles, *Tetrahedron* **68**: 2743-2757 (2012).

[5] Suresh Maddilaa, Satya Kumar, Avula Anil, Kumar Avula PalakonduLavanya., Efficient Organocatalytic Multicomponent Synthesis of (α-aminoalkyl) phosphonates, *Arabian Journal of Chemistry*, **9**: 787-791 (2016).

[6] Sienczyc M., Oleksyszyn., Irreversible Inhibition of Serine Proteases - Design and in Vivo Activity of Diaryl Alpha-Aminophosphonate Derivatives, *J. Curr. Med. Chem*., **16**: 1673 – 1687 (2009).

[7] Long N., Cai X.J., Song B.A., Yang S., Chen Z., Bhadury P.S., Lu D.Y., Jin L.H., Xue W., A Study the Kabachnik–Fields Reaction of Benzaldehyde, Cyclohexylamine, and Dialkyl Phosphites, *J. Agric. Food*. **56**: 5242- 5250 (2008).

[8] Wang Q., Zhu M., Zhu R., Lu L., Yuan C., Xing S., Fu X., Mei Y., Hang Q., Exploration of α-aminophosphonate N-derivatives As Novel, Potent and Selective Inhibitors of Protein Tyrosine Phosphatases., *Eur. J. Med. Chem*. **49**: 354- 364 (2012).

[9] S. Dake A., Raut D.S., Kharat K.R., Mhaske R.S., Deshmukh S.M., Pawar R., Ionic Liquid Promoted Synthesis, Antibacterial and in vitro Antiproliferative Activity of Novel A-Aminophosphonate Derivatives, P., *Bioorg. Med. Chem. Lett.*, **21**: 2527-2532 (2011).

[10] K. Huang B., Chen Z.F., Liu Y.C., Li Z.Q., Wei J.H., Wang M., Xie X.L., Liang H., Platinum(II) Complexes with Mono-Aminophosphonate Ester Targeting Group that Induce Apoptosis Through G1 Cell-Cycle Arrest: Synthesis, Crystal Structure and Antitumour Activity, *Eur. J. Med. Chem.* **64**: 554-562 (2013).

[11] Domingo L.R., Pérez P., Global and Local Reactivity Indices for Electrophilic/ Nucleophilic Free Radicals, *Organic & Biomolecular Chemistry*, **11(26)**: 4350-4359 (2013).

[12] Abdel Halim S., Ibrahim M.A., Synthesis, Density Functional Theory Band Structure Calculations, Optical, and Photoelectrical Characterizations of the Novel (9-Bromo-3-cyano-5-oxo-1,5-dihydro-2H-chromeno[4,3-b] pyridin-2 ylidene) propanedinitr, *J. Heterocyclic Chem.* **56:** 2542-2554 (2019).

[13] Abdel Halim S., Laila I. Ali, Sameh Gamal Sanad., Theoretical Calculations of Solvation 12-Crown-4 (12CN4) in Aqueous Solution and its Experimental Interaction with Nano CuSO4, *Int. J. Nano Dimens.*, **8:** 142-158 (2017).

[14] Abdel Halim S., Ali Kh. Khalil., TD-DFT Calculations, NBO Analysis and Electronic Absorption Spectra of Some Thiazolo[3,2-a] pyridine Derivatives, *J. Mol. Struct.* **1147:** 651-667 (2017).

[15] (a) Becke A.D., A New Mixing of Hartree–Fock and Local Density-Functional Theories, *J. Chem. Phys.* **98**: 1372-1376 (1993).
(b) Becke A.D., Density Functional Thermochemistry, III: The Role of Exact Exchange, *J. Chem. Phys.* **98**: 5648-5652 (1993).

[16] (a) Lee C., Yang W., Parr R.G., Development of the Colle-Salvetti Correlation-Energy Formula into a Functional of the Electron Density, *Phys. Rev. B Condens Matter*, **37**: 785-789 (1988).
(b) Miehlich B., Savin A., Stolt H., Preuss H., Results Obtained with the Correlation Energy Density Functional of Becke and Lee, Yang and Parr, *Chem. Phys. Lett.*, **157**: 200-206 (1989).

[17] Stefanov B., Liu B.G., Liashenko A., Piskorz P., Komaromi I., Martin R.L., Fox D.J., Keith T., Al-Laham M.A., Peng C.Y., Nanayakkara A., Challacombe M., Gill P.M.W., Johnson B., Chen W., Wong M.W., Gonzalez C., Pople J.A., Gaussian, Gaussian Inc., Pittsburgh PA. (2003).

[18] Gaussian 09, Revision A.1, Frisch M.J., Trucks G.W., Schlegel H.B., Scuseria G.E., Robb M.A., Cheeseman J.R., Scalmani G., Barone V., Mennucci B., Petersson G.A., Nakatsuji H., Caricato M., Li X., Hratchian H.P., Izmaylov A.F., Bloino J., Zheng G., Sonnenberg J.L., Hada M., Ehara M., Toyota K., Fukuda R., Hasegawa J., Ishida M., Nakajima T., Honda Y., Kitao O., Nakai H., Vreven T., Montgomery J.A., Jr., J.E. Peralta, F. Ogliaro, Bearpark M., Heyd J.J., Brothers E., Kudin K.N., Staroverov V.N., Kobayashi R., Normand J., Raghavachari K., Rendell A., Burant J.C., Iyengar S.S., Tomasi J., Cossi M., Rega N., Millam J.M., Klene M., Knox J.E., Cross J.B., Bakken V., Adamo C., Jaramillo J., Gomperts R., Stratmann R.E., Yazyev O., Austin A.J., Cammi R., Pomelli C., Ochterski J.W., Martin R.L., Morokuma K., Zakrzewski V.G., Voth G.A., Salvador P., Dannenberg J.J., Dapprich S., Daniels A.D., Farkas O., Foresman J.B., Ortiz J.V., Cioslowski J., Fox D.J., Gaussian, Inc., Wallingford CT, (2009).

[19] GaussView, Version 5, Dennington, R.; Keith, T.; Millam, J. Semichem Inc., Shawnee Mission K.S, (2009).

[20] http://www.chemcraftprog.com.

[21] Avci D., Second and Third-Order Nonlinear Optical Properties and Molecular Parameters of Azo Chromophores: Semiempirical Analysis, *Spectrochim. Acta. A*, **82**: 37-43 (2011).

[22] Avci D., Başoğlu A., Atalay Y., Ab initio HF and DFT Calculations on an Organic Non-Linear Optical Material, *Struct. Chem.*, **21**: 213-219 (2010).

[23]. Avci D, Cömert H., Atalay Y., Ab initio Hartree-Fock Calculations on Linear and Second-Order Nonlinear Optical Properties of New Acridine-Benzothiazolylamine Chromophores**,** *J. Mol. Mod.* **14**: 161-169 (2008).

[24] Matecki J.G.., Phosphoinositides: Tiny Lipids with Giant Impact on Cell Regulation, *Trans. Met. Chem*. **35**: 801-811 (2010).

[25] Yanai T., Tew D., Handy N.A., New Hybrid Exchange–Correlation Functional Was Using the Coulomb-Attenuating Method (CAM-B3LYP), *Chem. Phys. Lett.*, **393**: 51-57 (2004).

[26] Koopmans T., Über die Zuordnung von Wellenfunktionen und Eigenwerten zu den Einzelnen Elektronen Eines Atoms, *Physica*, **1(1-6)**: 104-113 (1934).

[27] Chocholoušová J., Špirko V., Hobza P., First Local Minimum of the Formic Acid Dimer Exhibits Simultaneously Red-Shifted O–H…O and Improper, Blue-Shifted C–H…O Hydrogen Bonds, *Phys. Chem.*, **6:** 37-41 (2004).

[28] Szafran M., Komasa A., Bartoszak-Adamska E., Crystal and Molecular Structure of 4-Carboxypiperidinium Chloride (4-piperidinecarboxylic acid hydrochloride), *J. Mol. Struct.* **827**: 101-107 (2007).

[29] Aranowska K., Graczyk J., Checinska L., Pakulska W., Ochocki., Antitumor Effect of Pt(II) Amine Phosphonate Complexes on Sarcoma Sa-180 in mice. Crystal Structure of Cis-dichlorobis(diethyl-4-pyridylmethyl- phosphonate-κN)platinum(II) hydrate, cis-[PtCl2(4-pmpe)2] · H2O, *J. Pharmazie*, **61**: 457- 460 (2006).

[30] Tarik Ali E., Salah A. Abdel-Aziz, Somaya M. El-Edfawy, El-Hossain A. Mohamed, Somaia M. Abdel-Kariem., Synthesis and Biological Evaluations of a Series of Novel Azolyl, Azinyl, Pyranyl, Chromonyl and Azepinyl Phosphonates, *Heterocycles*, **87:** 2513-2532 (2013).

[31] Tarik Ali E., Salah A. Abdel-Aziz, Somaya M. El-Edfawy, El-Hossain A. Mohamed, Somaia M. Abdel-Kariem., Cleavage of Diethyl Chromonyl α-Aminophosponate with Nitrogen and Carbon Nucleophiles: A Synthetic Approach and Biological Evaluations of a Series of Novel Azoles, Azines, and Azepines Containing α-Aminophosphonate and Phosphonate Groups, *Synthetic Communications*, **44**: 3610-3629 (2014).

[32] Lide D.R., A Survey of Carbon-Carbon Bond Lengths, *Tetrahedron.* **17**: 125-134 (1962).

[33] Reed A.R., Weinstock R.B., Weinhold F., Natural Population Analysis, *J. Chem. Phys.*, **83**: 735-745 (1985).

[34] Natorajan S., Shanmugam G., Martin S.A., *Cryst. Res. Technal.* **43** (2008) 561 D.S. Chemia, J. Zysss, Orlando, FL, (1987) Bradshow D.S., Andrews D.L., Electronic Structure, Biological Activity, Natural Bonding Orbital (NBO) and Non-Linear Optical Properties (NLO) of Poly-Functions Thiazolo [3,2-a] Pyridine Derivatives. DFT Approach, *J. Nonlinear Opt. Phys. Matter*, **18**: 285 – 295 (2009).

[35] Cheng L.., Tam W., Stevenson S.H., G. Meredith.R., Rikken G., Marder S.R., Experimental Investigations of Organic Molecular Nonlinear Optical Polarizabilities. 1. Methods and Results on Benzene and Stilbene Derivatives, *J. Phys. Chem.*, **95**: 10631-10643 (1991).

[36] Kaatz P., Donley E.A., Shelton D.P., A Comparison of Molecular Hyperpolarizabilities from Gas and Liquid Phase Measurements, *J. Chem. Phys.*, **108**: 849-856 (1998).

[37] Gnanasambandan T., Gunasekaran S., Seshadri S., Experimental and Theoretical Study of P-Nitroacetanilide, *Spectrochimica. Acta Part A: Molecular and Biomolecular Spectroscopy*, **117**: 557-567 (2014).

[38] Murray J.S., Sen K., Molecular Electrostatic Potentials, Conseptsana Applications, Elsevier, Amsterdam, (1996) 7 and E. Sscrocco, J. Tomasi, An Euristic Interpretation TD-DFT Calculations, NBO, NLO Analysis and Electronic Absorption Spectra of Some Novel Thiazolo[3,2-a] Pyridine Derivatives Bearing Anthracenyl Moiety, *Adv. Quant. Chem.* **11:** 115-135(1978).

[39] Politzer P., Murray J.S., The Fundamental Nature and Role of the Electrostatic Potential in Atoms and Molecules, *Theor. Chem. Acc.*, **108**: 134-142 (2002).

[40] Sajan D., Joseph L., Vijayan N., Karabacak M., Natural Bond Orbital Analysis, Electronic Structure, Non-Linear Properties and Vibrational Spectral Analysis of L-Histidinium Bromide Monohydrate: A Density Functional Theory, *Spectrochim. Acta A*, **81**: 85-98 (2011).

[41] Ditchfield R., Molecular Orbital Theory of Magnetic Shielding and Magnetic Susceptibility, *J. Chem. Phys.*, **56**: 5688–5691 (1972).

[42] Wolinski K., Hinton J.F., Pulay P., Efficient Implementation of the Gaugeindependent Atomic Orbital Method for NMR Chemical Shift Calculations, *J. Am. Chem. Soc.* **112**: 8251–8260 (1990).

[43] Kalinowski H.O., Berger S., Braun S., "Carbon-13 NMR Spectroscopy", John Wiley & Sons Inc., Chicheser, (1988).

[44] Lambert J.B., Shurvell H.F., Vereit L., Cooks R.G., Stout G.H., "Organic Structural Analysis", Academic Press, New York, (1976).

[45] Kalsi P.S., "Spectroscopy of Organic Compounds", Academic Press, New York, (2002).